Lithospheric Controls on Melt Production During Continental Breakup at Slow Rates of Extension: Application to the North Atlantic

J. J. Armitage,[12] T. J. Henstock,[1] T A. Minshull,[1] and J. R. Hopper,[3]

J. J. Armitage, Department of Earth Science and Engineering, Imperial College London, South Kensington Campus, London SW7 2AZ, UK. (j.armitage@imperial.ac.uk)

T. J. Henstock, National Oceanography Centre, Southampton, University of Southampton, European Way, Southampton SO14 3ZH, UK. (then@noc.soton.ac.uk)

T. A. Minshull, National Oceanography Centre, Southampton, University of Southampton, European Way, Southampton SO14 3ZH, UK. (tmin@noc.soton.ac.uk)

J. R. Hopper, Department of Geology and Geosciences, Texas A&M University, College Station, Texas 77843, USA. (hopper@geo.tamu.edu)

[1]National Oceanography Centre,
Southampton, University of Southampton,
UK

[2]Department of Earth Science and
Engineering, Imperial College London, UK

[3]Department of Geology and Geosciences,
Texas A&M University, College Station,
Texas, USA

Abstract. Rifted margins form from extension and breakup of the continental lithosphere. If this extension is coeval with a region of hotter lithosphere, then it is generally assumed that a volcanic margin would follow. Here we present the results of numerical simulations of rift margin evolution by extending continental lithosphere above a thermal anomaly. We find that unless the lithosphere is thinned prior to the arrival of the thermal anomaly or half spreading rates are more than $\sim \quad 50\,\mathrm{mm\,yr^{-1}}$, the lithosphere acts as a lid to the hot material. The thermal anomaly cools significantly by conduction before having an effect on decompression melt production. If the lithosphere is thinned by the formation of extensional basins then the thermal anomaly advects into the thinned region and leads to enhanced decompression melting. In the North Atlantic a series of extensional basins off the coast of northwest Europe and Greenland provide the required thinning. This observation suggests that volcanic margins that show slow rates of extension, only occur where there is the combination of a thermal anomaly and previous regional thinning of the lithosphere.

1. Introduction

Previous kinematic and dynamic models of continental rifting and associated melt production tend to consider a relatively simple rifting history of constant divergent extension (for example *Bown and White*, 1995; *Boutilier and Keen*, 1999; *Nielsen and Hopper*, 2004). However the history of many regions is more complicated, for example: the North Atlantic during the late Mesozoic saw multiple phases of rifting (e.g. *Doré et al.*, 1999); or, the Newfoundland-Iberia margin, which underwent multiphase rifting [*Reston*, 2007].

These geophysical observations show that caution must be used when applying simple geodynamic models to rifted margin formation. When modelling the formation of a rifted margin, some pre-thinning (*necking region*) of the lithosphere is often assumed (for example *Keen and Boutilier*, 2000; *Nielsen and Hopper*, 2004). This has been justified as it encourages small scale convection and focuses the melting at the ridge axis [*Boutilier and Keen*, 1999]. *Nielsen and Hopper* [2004] argued that the presence of such a numerical device makes little difference when there is no thermal anomaly present. In this article we will examine the effect of pre-thinned lithosphere on both the volume and chemistry of melt produced during rifting with and without thermal anomalies in the upper mantle. We will go on to investigate the relationships between this modelling device and a more complex multi-phase rifting history, using the North Atlantic as a study region.

The North Atlantic Ocean opened in a succession of extensional basins that finally ended with rifting leading to the North Atlantic Igneous Province. Prior to the rifting of the North Atlantic ~ 60 Ma ago, at the conjugate southeast Greenland margin and Hatton Bank system, there were up to three phases of extension. These lead to the formation of the Rockall Trough (120-300 Ma; *Smythe*, 1989; *Shannon*, 1991), the Hatton-Rockall Basin (~ 80 Ma; *Edwards*, 2002), and an extensional basin off the Southeast Greenland

margin prior to the eruption of the main phase of flood basalts [*Larsen and Saunders*, 1998].

The mechanisms that led to the formation of these flood basalts, which form part of the North Atlantic large igneous province (NAIP), remain contentious. Models that invoke edge-driven convection, small-scale convection or thermal anomalies are able to explain aspects of the formation of the NAIP (see *Meyer et al.*, 2007). Edge-driven convection, where a change in thickness from young (normal) to old (cratonic) continental lithosphere, will generate a convection cell [*King and Anderson*, 1998]. But it is likely that this convection alone will not generate significant amount of melt, as it will not penetrate the young lithosphere [*Nielsen and Hopper*, 2004; *Sleep*, 2007]. Likewise, models that appeal to buoyant upwelling of mantle material due to melt generation alone cannot explain the increased crustal thickness observed at the Southeast Greenland and Hatton Bank margins (e.g. *Nielsen and Hopper*, 2004; *Simon et al.*, 2009). In this study we will therefore include the effects of buoyant upwelling, thermal anomalies and the topography of the base of the lithosphere.

Armitage et al. [2008] found that the history of melt production at the Southeast Greenland margin could be explained by rifting above a 50 km thick 200 °C thermal anomaly, with initial half spreading rates of $40\,\mathrm{mm\,yr^{-1}}$. Within the first few million years after breakup the half spreading rates then reduced to $10\,\mathrm{mm\,yr^{-1}}$. This period of fast extension has recently been questioned by *White and Smith* [2008], as there is no evidence for fast extension on the conjugate Hatton margin. Furthermore, the authors question the identification of magnetic cryptochrons (see *Larsen and Saunders*, 1998) on which this period of fast extension is based. Our previous model of the Southeast Greenland margin repro-

duced the igneous thickness observed, however it also relied upon the same pre-thinning of the lithosphere as *Keen and Boutilier* [2000] and *Nielsen and Hopper* [2004].

We will show that a thinned lithosphere is required to match the observations. Furthermore, the earlier phases of extension in the North Atlantic have the required effect of thinning the lithosphere. This pre-extension history may also resolve some of the apparent asymmetry between the Southeast Greenland margin and Hatton Bank.

2. Methods

We employ the model developed in *Armitage et al.* [2008], which is based upon *Citcom* [*Moresi et al.*, 1996; *Nielsen and Hopper*, 2004]. The lithospheric mantle is assumed to deform in a viscous manner by Stokes Equations,

$$\frac{\partial u_i}{\partial x_i} = 0 \tag{1}$$

$$-\frac{\partial \tau_{ij}}{\partial x_j} + \frac{\partial p}{\partial x_i} = \Delta\rho g \lambda_i \tag{2}$$

$$\frac{\partial T}{\partial t} = -u_i \frac{\partial T}{\partial x_i} + \kappa \frac{\partial^2 T}{\partial x_j^2} - \frac{L\dot{m}}{c_p} \tag{3}$$

where repeated indices are summed. u is the solid mantle creep, T is the mantle temperature, τ is the deviatoric stress tensor, $\Delta\rho$ is the density change due to temperature and the generation of melt, $\dot{m}$ is the melt production rate, g is the acceleration due to gravity and λ_i is a unit vector in the vertical direction (*i.e.* $\lambda_1 = 0$, $\lambda_2 = 1$). The other constants are defined within Table 1. The deviatoric stress is given by,

$$\tau_{ij} = 2\eta\dot{\epsilon_{ij}} \tag{4}$$

where $\dot{\epsilon_{ij}}$ is the strain rate and η is the viscosity given by the following rheological definition,

$$\eta = A\chi_{H_2O}\chi_m exp\left(\frac{E+pV}{nRT}\right)\dot{\epsilon}^{\frac{1-n}{n}} \tag{5}$$

where E is the activation energy, V is the activation volume, n is the stress exponent and R is the gas constant. A is a rheological parameter set from the reference state of $T = 1598\,^{\circ}\mathrm{C}$, $\eta = 4.5 \times 10^{20}\,\mathrm{Pa\,s}$ and $\dot{\epsilon} = 1 \times 10^{-15}\,\mathrm{s}^{-1}$. The rheological definition has two further terms to account for the strengthening of the mantle due to the removal of mantle volatiles χ_{H_2O}, and the weakening of the mantle due to small amounts of melt, melt weakening, χ_m as defined in *Nielsen and Hopper* [2004].

The mantle convection is governed by the density variation, $\Delta\rho$ in Equation 2, which is a function of melt generation and temperature (see *Nielsen and Hopper*, 2004). The melt depletion is tracked using the melt residue as defined by *Scott* [1992]. The melt residue, X, increases as melting progresses. It is similar to the concentration of a completely incompatible trace element, in that its concentration increases as melting progresses. X increases from 1 as melting increases. It can be related to the amount of melt fraction,

$$F = \frac{M}{M_0} \tag{6}$$

where M is the mass of melt phase and M_0 is the initial total mass of unmelted mantle, by assuming within the melt region the melt and solid matrix remain well mixed such that [*Scott*, 1992],

$$X(1 - F) = 1 \tag{7}$$

The melt residue is advected following [*Scott*, 1992],

$$\frac{\partial X}{\partial t} + u_i \frac{\partial X}{\partial x_i} = \frac{X}{1 - \phi}\dot{m} \tag{8}$$

where ϕ is the melt porosity, which is subject to advection and compaction,

$$\frac{\partial \phi}{\partial t} + u_i \frac{\partial \phi}{\partial x_i} + (1 - \phi)\frac{\partial u_j}{\partial x_j} = \dot{m} \tag{9}$$

The melt production is calculated at each time step from,

$$\delta m = \frac{\delta t}{\frac{L}{c_p} + \frac{\partial T_s}{\partial \phi}} \tag{10}$$

where $\delta T = T - T_s$ and T_s is the wet or dry solidus temperature. The solidus is defined as being dependant on the melt residue, X, and pressure following *Scott* [1992] and *Phipps Morgan* [2001],

$$T_s^{dry} = T_{s0} + z\left(\left(\frac{\partial T_s}{\partial z}\right)_X - \left(\frac{\partial T}{\partial z}\right)_S\right) + \left(\frac{\partial T_s}{\partial X}\right)_z (X - 1) \tag{11}$$

The depth derivative of the solidus at constant depletion $(\partial T_s/\partial z)_X$ is assumed to be $3.4 \times 10^{-3}\,\mathrm{K\,m^{-1}}$ [*Scott*, 1992]. The depletion derivative of the solidus at constant depth $(\partial T_s/\partial X)_z$, or solidus-depletion gradient is assumed to be $200\,^{\circ}C$ [*Scott*, 1992]. The wet solidus is given by,

$$T_s^{wet} = T_s^{dry} - \Delta T_s \frac{1.02 - X}{\Delta X} \tag{12}$$

where wet melting occurs until a melt fraction of 2 %, $\Delta X = 0.02$, is generated, or depletion $X = 1.02$. Then the mantle is assumed to be dry, and the solidus shifts to the dry solidus, defined in Equation 11. The latent heat capacity in Equation 10 is given by $L = T_s \Delta S$, where ΔS is the entropy change due to melting and c_p is the specific heat capacity (see Table 1). The differential $\partial T_s/\partial \phi$ is given by, when in the wet melting regime (from *Nielsen and Hopper* [2004]),

$$\frac{\partial T_s}{\partial \phi} = 1440 \frac{X}{1 - \phi} \tag{13}$$

and when in the dry melting regime,

$$\frac{\partial T_s}{\partial \phi} = 440 \frac{X}{1 - \phi} \tag{14}$$

Therefore the melt production rate is simply,

$$\dot{m} = \frac{\delta m}{\delta t} \tag{15}$$

where δt is the advection time step. Melt production then couples the energy balance (Equation 3) and the advection of the melt residue, X. This allows for the calculation of the mean melt fraction, $\overline{F}$, defined in *Plank et al.* [1995] as the mean value of F in the pooled melts:

$$\overline{F} = \frac{\int\int F\dot{m}dxdz}{\int\int \dot{m}dxdz} \tag{16}$$

Igneous crustal thickness h_c is calculated following *Ito et al.* [1996],

$$h_c = \frac{2}{u_z}\left(\frac{\rho_m}{\rho_l}\right)\int\int_{melt}\dot{m}dxdz \tag{17}$$

Where the averages are over the melt region, u_z is the vertical velocity at the ridge axis, ρ_m is the density of the lithospheric mantle and ρ_l is the melt density (see Table 1).

The model space is a region 2800 km long by 700 km deep of upper lithosphere and mantle. Mantle potential temperature is chosen to be 1325 °C such that the final steady-state melt production yields a crustal thickness of 8–11 km, consistent with the North Atlantic [*Armitage et al.*, 2008; *Nielsen and Hopper*, 2004]. Boundary conditions are of free slip except at the top where spreading is imposed, and of no flow across the boundary. The bottom and side boundaries are kept far from the melting region to minimise the impact of these boundary conditions on the evolving system.

Models are set up with a 125 km thick, buoyant and cool lithosphere, with a thermal anomaly below (Figure 1). The thermal anomaly is included to simulate an exhaustible layer of hot mantle that generates the enhanced breakup magmatism as seen off the Southeast coast of Greenland, the Vøring Plateau, Hatton Bank and the Edoras Bank [*Barton and White*, 1997; *Holbrook et al.*, 2001; *Mjelde et al.*, 2005; *Voss and Jokat*, 2007; *White et al.*, 2008].

We use the parametrisation of *Niu* [1997] to calculate the major element primary composition of the melts from the melt fraction, temperature and pressure within the melt

region. The *Niu* [1997] parametrisation does have limitations at low melt fractions and at high pressures [*Armitage et al.*, 2008]. Yet this parametrisation can recreate MORB reasonably and it can track the depletion of the mantle as melting progresses [*Armitage et al.*, 2008; *Dean et al.*, 2008]. We then average the melt composition for each time step over the whole melt region (*melt*), following *McKenzie and Bickle* [1988],

$$\overline{C} = \frac{\int\int_{melt} FC dx dz}{\int\int_{melt} F dx dz} \tag{18}$$

This is critical to understand the consequences of multiphase rifting events on melt production and chemistry. Although the melting characteristics include wet melt production, the composition parametrisation does not. Since water is assumed to be removed by the time the melt fraction reaches 2 % any errors in predicted compositions will be small.

The thermal anomaly associated with the North Atlantic igneous province is in the range of 50 to 250 °C hotter than the mantle [*Holbrook et al.*, 2001; *White and McKenzie*, 1989]. Recent geodynamic modelling of a laterally spreading thermal plume has found that the North Atlantic thermal anomaly was likely between 50 and 100 km thick [*Nielsen and Hopper*, 2002]. Similarly, modelling of a layer of hot exhaustible material of variable thickness has found that, for the North Atlantic, this anomaly was likely 50 km thick [*Keen and Boutilier*, 2000]. As we are interested in applying our model to the Southeast Greenland margin, we will explore the consequences of the thermal anomaly being either 100 km or 50 km thick.

3. Results and Discussion

3.1. Single Phase Rifting Events

We begin with simple simulations of a hypothetical symmetric rift system. Five cases of extension are considered: *Case 1* has no thermal anomaly and no necking region imposed. This is the base model against which comparisons will be made. *Case 2* has a

200 °C, 50 km thick hot layer beneath the 125 km thick lithosphere, but still no necking region imposed. *Case 3* increases the thickness of the hot layer to 100 km keeping the temperature the same. *Case 4* is as case 1 but with an added necking region, and *Case 5* is as case 2 but with a necking region. First cases 1, 2 and 3 are compared. Then we shall impose the necking region and compare cases 4 and 5, finally making some general comments of the difference between all five cases.

3.1.1. Models With no Necking Region: Cases 1, 2 and 3

Case 1 represents background stretching with no pre-thinning, flat lithosphere, and no thermal anomalies. Rifting of the lithosphere under these conditions gives a margin that evolves through a gradual thickening of igneous material after breakup, with a gradual depletion in TiO_2, Na_2O and little to no variation in MgO (Figure 2). This reflects low melt fractions within the melt region. Increased volumes of material arise from the expansion of the melt region only, as the melt region evolves to the steady state triangular region as expected under a mid-ocean ridge. Addition of a 200 °C thermal anomaly within the model of rifting (case 2; Figure 2) has the effect of increasing the early igneous crustal thickness, making the continent to ocean transition more rapid, as suggested by *Nielsen and Hopper* [2004].

The peak in melt production in case 2, reflected in igneous thickness, at fast spreading rates is an effect of the hot layer in this case: FeO and MgO enrichment reflect high melt fractions (Figure 2). Thickened crust upon breakup is a reflection of the size of the melt region and of high melt fractions within the melting region. In the fast spreading case FeO concentrations peak due to the formation of deep melts, then as the thermal anomaly rises the MgO concentration peaks reflecting high melt fractions (Figure 2). Peaks are also observed in the model of slow extension, but diminished and much delayed.

The thermal anomaly must be advected to shallower regions if it is to influence melt generation; this hot layer however loses heat by conduction to the cooler surroundings. Thus for the hot layer to give enhanced melt production, it must move into the melting region before cooling significantly, on a timescale of less than 20–25 Myr for a layer 50 km in thickness. At slow spreading rates, the extension and thinning of the lithosphere is sufficiently slow that although case 2 does have increased melt production from 5–20 Myr over case 1, the igneous thickness never significantly exceeds the steady-state value (Figure 2). The thermal anomaly decays by conduction before the steady-state melting is established. At the faster spreading rates thinning of the lithosphere is sufficient to bring the thermal anomaly into the melt region and cause significant excess melt production. Conversely, a 100 km thick hot layer does persist for long enough to cause excess melting even at slow rifting rates (Figure 3).

By increasing the thickness of the thermal anomaly to 100 km (Case 3), greater amounts of melt are generated. A thicker hot layer introduces a sustained peak in igneous thickness and upwelling at all spreading rates. The thicker thermal anomaly broadens the region of lithosphere thinning and so slightly reduces the velocity of material upwelling within the melting region (Figure 3). The excess melt production when the thermal anomaly is 100 km thick however lasts up to 30 Myrs (Figure 3). The models indicate that a simple 1-D exhaustible hot layer is insufficient to generate high transient syn-rift melt thicknesses at slow spreading rates: either the anomaly will cool before having a significant effect on the melting region, or it will produce excess melt for an extended period of time.

3.1.2. Models With an Imposed Necking Region: Cases 4 and 5

Within the final sets of simulations, a narrow pre-thinned region at the centre of extension has been included as an initial condition. This thinned region is triangular in

shape with a half width of $\sim 25\,\mathrm{km}$ [*Nielsen and Hopper*, 2004] and is similar to that used by *Keen and Boutilier* [2000]. The hot layer is not assumed to have advected into this narrow region prior to rifting. The evolution without and with a 50 km 200 °C hot layer beneath the lithosphere (case 4 and 5) is tested. The most obvious outcome is that rifting above a thermal anomaly leads to thickened crust at all spreading rates (Figure 4). Yet if Figures 2 and 4 are compared, the pre-thinning has had the clear effect of increasing the melt generation during early rifting.

The presence of the pre-thinned region in combination with a thermal anomaly has a far greater effect on the volumes of material generated than when there is not a pre-thinned region (Figure 6). Upon the pulse of increased melt production there is a peak of enrichment of FeO and MgO, and increased depletion in TiO_2 and Na_2O (Figure 4). This reflects the presence of early deep melt combined with slightly later shallow and high ($\sim 18\,\%$) melt fractions. This is not the major effect though: the upwelling ratio, the ratio between the mean upwelling velocity in the melting region and the half spreading rate, is greatly enhanced by the thinned lithosphere causing more focussed extension, resulting in greatly enhanced melt production. The pre-thinned initial condition reduces the viscosity of the upper lithosphere as the viscous lid has been extended and replaced by asthenospheric mantle at the outset. The lower viscosity together with the stronger lateral thermal gradients provide the best conditions for transient small-scale convection. This, together with the higher temperatures within the melting region, leads to a more rapid onset of melt production. The models indicate that if an exhaustible thermal anomaly is to have a large but transient effect on the melt generation at slow spreading rates it must be combined with some pre-thinning of the lithosphere. In the next section we will

explore the consequence of thinning modelled in a consistent manner due to extension, rather than by imposing a necking region.

Without the presence of a thermal anomaly, the pre-thinned model (case 4) has a significantly increased upwelling velocity compared to the half spreading rate (Figure 5). The pre-thinned region focuses flow upon breakup, which increases the igneous crustal thickness more rapidly as the model evolves. When there is no thermal anomaly present, however the onset of significant melting is merely delayed [*Nielsen and Hopper*, 2004]. From the profiles of igneous thickness, the flat lithosphere model (case 1) extends for 14 Myrs before significant crust is generated, which is much delayed when compared to the pre-thinned model (case 4).

The melt production characteristics of case 1 at a slow half spreading rate of $10\,\mathrm{mm\,yr^{-1}}$ shows a resemblance margins where there is a lack of excess magmatism (Figure 5). Modelling with one-dimensional heat flow suggested that the rate of spreading should be ultra slow ($< 10\,\mathrm{mm\,yr^{-1}}$) for melting to be suppressed significantly at a rifted margin [*Bown and White*, 1995]. Here, our model which includes two-dimensional heat flow shows that even at $10\,\mathrm{mm\,yr^{-1}}$ lateral conduction of heat can help to suppress significant decompression melting.

3.2. Multiphase Rifting Events

Multiphase rifting events occur when the lithosphere is subject to extension prior to the eventual rifting and transition to sea floor spreading. The centre of extension may then subsequently shift by small jumps or migration. As the lithosphere is extended, its strength initially decreases and if the strain rates are high enough the extension will lead to breakup [*England*, 1983]. However, if extension is slow then the centre of that extension may shift through time due to a strengthening of the lithosphere as it cools

during extension [*Houseman and England*, 1986; *Bassi et al.*, 1993]. This will lead to a succession of extensional basins, such as observed of the west coast of Norway, which precede the eventual breakup [*van Wijk and Cloetingh*, 2002].

Ridge jumps may also be the consequence of the arrival of a plume head. The plume will erode the lithosphere by the advection of material due to the buoyant upwelling of the new hot material [*Jurine et al.*, 2005]. Re-localisation of the centre of extension may then be encouraged by the eventual penetration of plume material through the crust [*Mittelsteadt et al.*, 2008]. We will however impose ridge jumps, as we wish to explore the consequences of such jumps on melt volumes rather than the reasons for ridge jumps. The possible reasons for ridge jumps are outside the scope of our model.

Within our model the lithosphere is initially of a constant 125 km thickness (Figure 7). We then subject the lithosphere to a divergent velocity boundary at between 5 and 50 mm yr^{-1}, which leads to thinning of the continental lithosphere. This process simulates the effect of prior periods of extension near to the subsequent rift region in a way which is physically consistent with the remainder of the model. The centre of extension is then shifted by 44, 88, 175, or 350 km to simulate ridge jumps. The rift forms above a 50 km thick 200 °C thermal anomaly.

We will initially explore melt production sensitivity to the distance of simulated ridge jumps and the degree of extension undergone in the extensional basins. The extensional basins are stretched by factors of between 1.1 and 9, at half spreading rates between 5 and 50 mm yr^{-1}. Finally the effect of passive conductive cooling between the prior extension and rift will be simulated.

3.2.1. Rifting at Increasing Distances From Pre-thinning Event

In these simulations rifting occurs in two stages: an initial period of extension that may lead to a failed rifted margin. This is followed by the migration of the centre of extension forming a second rifted margin, which is associated with the arrival of the hot layer, leading finally to the breakup of the continental lithosphere. To explore the impact of rift migration, we have made the simplifying assumption that the initial period of extension is very slow (Figure 9a). The half spreading rate during the first period of extension is $5\,\mathrm{mm\,yr^{-1}}$ and the second period of extension is at $10\,\mathrm{mm\,yr^{-1}}$, with the addition of the hot layer (Figure 8). These half spreading rates were chosen to minimise the effects of melting within the first failed rift. In addition, if the half spreading rates are fast then the lithosphere is thinned rapidly allowing the advection of hot material into the melting region (see Case 2; Figure 2). Extension in the first failed rift is by a factor of between 1.1 and 9 before the arrival of the thermal anomaly. Extension then is shifted away from the failed rift.

The thinning of the lithosphere in the first stage of extension, if close enough to the new centre of extension, acts in similar manner to the artificial necking region imposed in Section 3.1.2: the hot layer is advected into the area that has undergone prior extension if this is nearby (Figure 8). Increasing the distance of the migration between the two extensional events reduces the melt production and peak igneous thickness during breakup (Figure 9a). The reasons are as outlined previously: for a thin thermal anomaly to have an impact on the melting characteristics it needs a region of previously thinned lithosphere. As the rift event jumps successively further from the previously-thinned region that event has progressively less influence. If the first period of extension is less than a factor of ~ 3, then the subsequent rift will generate only a modest 2 km increase in igneous crustal

thickness. For larger degrees of extension, the peak igneous crustal thickness reaches $\sim 13\,\mathrm{km}$ (Figure 9a).

As the half spreading rate of the first period of extension is increased, from $5\,\mathrm{mm\,yr^{-1}}$ to $50\,\mathrm{mm\,yr^{-1}}$, the peak igneous thickness from the second stage of extension is increased (Figure 9b). There are two competing processes: first there is the thinning of the lithosphere during the initial extension event that leads to enhanced melting. Second, there is depletion of the upper lithosphere due to prior melting during the initial extensional event. At slow spreading rates the volumes of melt generated are very small. With a half spreading rate of between 5 and $20\,\mathrm{mm\,yr^{-1}}$ the degree of extension is the main control on peak igneous thickness (Figure 9b). It is only when the lithosphere is extended rapidly during the first extension phase that depletion of the mantle begins to affect melt production during the second extension phase. The primary control, therefore, on melt production during rifting other than the presence of the thermal anomaly, is the proximity between the failed and successful margin. Of secondary consideration is the spreading rate of the initial extensional phase, as this controls the width of the base of the thinned region prior to rifting.

3.2.2. Emplacement of the Thermal Anomaly

We have assumed that the thermal anomaly is similar to that postulated by *Keen and Boutilier* [2000]: a horizontal layer of warm material of uniform thickness at a fixed depth. This thermal anomaly rapidly rises to fill the thinned region of the lithosphere (Figure 8). If this thermal anomaly is plume related, then it has been postulated that the hot material would flow along the base of the lithosphere following the sublithospheric topography (*Sleep*, 1996; Figure 10). Hot material may also pond beneath thinned regions of the lithosphere (*Sleep*, 1996; Figure 11). To explore the consequences of how this hot

material is emplaced, we have compared the evolution of a two stage rift with an initial period of extension at a half spreading rate of $5\,\mathrm{mm\,yr^{-1}}$ that lasts 17 Myrs leading to extension by a factor of 5. Then as in Figure 8, the centre of extension then shifts by 44 km and then extension is at a half spreading rate of $10\,\mathrm{mm\,yr^{-1}}$.

Assuming that emplacement of the hot mantle occurs rapidly, then if the hot layer simply follows the sublithospheric topography melt generation is reduced (Figure 12). We refer to this emplacement scenario as the *drape* model. The reduction in melt generation is due to the hot material effecting a smaller portion of the melt region, rather than being vertically advected through the melt region (compare Figures 8 and 10). If the hot material were to pond beneath the thinned region of lithosphere then the thickness of the thermal anomaly is effectively increased. Assuming that the ponded hot material extends to 175 km (Figure 11) then 16 km compared 13 km of igneous crust is generated (Figure 12).

Therefore the configuration of the thermal anomaly can have a further effect on the subsequent melt generation during rifting. We have assumed that ponding is very rapid and so hot material does not advect into the thinned region. We would expect the hot material to melt due to decompression as it flows into the region beneath the thinned lithosphere. In the following section we will allow for the thermal anomaly to advect into the thinned region of the lithosphere, as such a scenario is perhaps more realistic than instantaneous ponding.

3.2.3. Rifting After an Increasing Period of Time

During the ridge jump there may be a period where extension is accommodated elsewhere, so the rift region has no activity. By removing all kinematic boundary conditions of spreading within our model the lithosphere cools by passive conduction. This causes

the thinned region of lithosphere to thicken by thermal conduction. The peak igneous thickness of the subsequent successful rifted margin reduces by approximately 1 km per 10 Myrs of cooling. Therefore if the lithosphere was extended by a factor of eight and if no extension occurs for 70 Myrs, then cooling will have returned the lithosphere to its original thickness. The subsequent rifted margin would then only generate 7 km of igneous crust. If the the extension of the first failed rift was around two, then the time taken to remove the thermal thinning of the base of the lithosphere would be less, at around 30 Myrs.

The time taken to remove the effect of the initial period of extension is dependant on the rate of conductive cooling. Cooling of the lithosphere will be modified by internal heating within due to radioactive decay. Internal heat production has not been included within these simulations. The heat flux generated by radioactive decay is greater within the upper and lower crust than at depth within the mantle [*McKenzie et al.*, 2005]. This internal heat production increases the temperature of the geotherm, particularly at the base of the lithosphere, where the thermal regime goes from being mainly controlled by heat conduction to convection. If the distribution of the internal heat is concentrated towards the lower crust, then temperatures within the thermal boundary layer at the base of the lithopshere can be significantly increased, effectively thinning the lithosphere [*Cooper et al.*, 2004]. It is therefore likely that heat production due to radioactive decay will prolong the preservation of thin regions of the lithosphere.

4. Application to the Opening of the North Atlantic

4.1. Extensional Basins offshore UK, Ireland and Southeast Greenland

The North Atlantic underwent a series of extensional events prior to the transition from rift to oceanic crust at the Paleocene-Eocene boundary (around 56 Ma; *Storey et al.*, 2007). Off the western shores of Ireland lies the Rockall-Hatton Plateau. The Rockall

Trough separates this fragment of continental continental crust from Ireland (Figure 13). The formation of the Rockall Trough may have initiated as early as the Carboniferous [*Smythe*, 1989]. It is thought that extension within this basin continued through out Mesozoic, with the youngest phase of rifting being the early Cretaceous (around 120 Ma; *Shannon*, 1991). The Rockall Trough is therefore too old to leave a significant thermal signature in the sublithospheric topography that would affect subsequent rifting at around 60 Myrs later.

The Rockall-Hatton Plateau consists of two highs, the Hatton and Rockall Banks (Figure 13). These are separated by a shallow sedimentary basin, which is called either the Hatton Basin [*Hitchen*, 2004], Hatton Trough [*Doré et al.*, 1999] or Hatton-Rockall Basin (*Shannon*, 1991; *Edwards*, 2002; 'HR Basin' in Figure 13). The Hatton-Rockall Basin was extended by a factor of two [*Smith et al.*, 2005]. It is separated from the region of eventual breakup by the Hatton Bank, which is close to 100 km wide at its widest point.

It has been suggested that the Hatton-Rockall Basin formed at a similar time as the Rockall Trough [*Smythe*, 1989]. *Edwards* [2002] argues that there is no direct evidence of this, and given the general lack of reversed polarity magnetic anomalies within the Hatton-Rockall Basin, instead suggests that it formed between 120 and 80 Ma. A younger age is also supported by a thin sedimentary sequence overlying the basement rock which may be Tertiary [*Shannon et al.*, 1993]. This leads *Doré et al.* [1999], to propose tentatively that rifting in the Hatton-Rockall Basin continued into the early Paleocene. Views on the age of extension in the Hatton-Rockall Basin are thus conflicting. We have made an assumption that rifting ceased during the Late Cretaceous, within 20 Ma of the earliest flood basalts on Southeast Greenland. This timing would mean that the sublithospheric

signature of this extensional event has the potential to impact the evolution of rifting in the North Atlantic.

Prebasaltic shallow marine sediments along the Southeast Greenland coast suggest the presence of Late Cretaceous to early Tertiary basins along this coastline (*Larsen*, 1980; *Larsen and Saunders*, 1998; Pre-rift basin in Figure 13). Analyses of sediments buried under the flood basalts at ODP site 917 have suggested that this pre-rift basin was similar to the Kangerlussuaq basin [*Larsen and Saunders*, 1998]. The authors further suggest that the basin likely formed just prior to the most early magmatism, at around 61 Ma. This pre-rift basin likely extended by only a small factor prior to breakup. The Kangerlussuaq basin subsided by ~ 700 m prior to 61 Ma [*Peate et al.*, 2003]. Assuming the instantaneous extension model of *McKenzie* [1978], to stretch the basin until a water loaded subsidence of 700 m would require extension by a factor of between 1.3 and 1.4. However instantaneous extension implies an infinite strain rate. If we assume that extension is at a half spreading rate of $10\,\mathrm{mm\,yr^{-1}}$, and taking an isostatic balance from the base of the lithosphere to the surface, to stretch the basin until a water loaded subsidence of 700 m would require extension factor of 1.1.

4.2. Results and Discussion of Models

The regional geology indicates that there are two extensional phases that will effect magmatism during final breakup: the Hatton-Rockall Basin and pre-rift basin (Table 2). This is a more complex scenario compared to the test simulations in the previous section, but the same principles should hold. The first and second phase of extension will thin the lithosphere, which may facilitate channelling of the distal plume material at 61 Ma and providing the required thermal anomaly (*Storey et al.*, 2007; Figure 13). Rapid emplacement of the hot layer is indicated, otherwise conductive cooling of the

emplaced material would suppress subsequent melt production. The hot material then advects upwards to fill the sublithospheric topography. The spreading rates chosen for the first two extension phases match the estimated stretching factors and the time periods for these phases (Table 2).

Previously we have argued for a period of fast extension, half spreading rates of $40\,\mathrm{mm\,yr^{-1}}$, during early breakup of the Southeast Greenland margin [*Armitage et al.*, 2008]. This period of fast extension is based on two sources. From the SIGMA III survey, making the assumption that the continent-ocean boundary (COB) is at 56 Ma and that the seaward dipping reflector series (SDRs) observed to the west of the COB are erupted on continental crust, the distance between the COB to C24n is around 100 km giving an average half spreading rate of $33\,\mathrm{mm\,yr^{-1}}$ [*Hopper et al.*, 2003]. This period of fast extension is backed up by the identification by *Larsen et al.* [1994] of magnetic anomalies between anomaly C24n and the COB that put half spreading rates at $44\,\mathrm{mm\,yr^{-1}}$.

However the interpretation of the magnetic lineations observed in the aeromagnetic survey as magnetic anomalies has been recently brought into question [*White and Smith*, 2008]. They suggest that these magnetic lineations are the edges of sub-horizontal lava flows. If so, then the fast initial rates of extension assumed by *Armitage et al.* [2008] may not represent accurately the formation of the Southeast Greenland margin. An alternative model is that the conjugate margin was symmetric and opened at initial half spreading rates of between 15 and $20\,\mathrm{mm\,yr^{-1}}$ [*Smallwood and White*, 2002; *White and Smith*, 2008]. Such a model resolves the conceptual difficulties with asymmetric spreading rates across the margin, though it does not explain the wide 100 km continent to ocean transition (COT) on the Southeast Greenland margin and narrow 40 km COT off the Hatton Bank [*Hopper et al.*, 2003; *White and Smith*, 2008].

To test the effect of the possible pulse of faster extension at breakup of the margin, we have modelled the two differing half spreading rates assuming that extension across the margin is symmetric. The prior extensional events have caused the lithosphere to thin asymmetrically prior to breakup (Figure 14). Numerical and analogue modelling of extension of the lithosphere have shown that asymmetries in the Moho can lead to asymmetric breakup and transition to sea floor spreading [*Corti and Manetti*, 2006; *Corti et al.*, 2003]. Here the asymmetric sublithospheric topography generated by the extension of the Hatton-Rockall Basin and the pre-rift basin causes a slight westward component to the mantle flow during breakup (~ 56 Ma, Figure 14). This asymmetric mantle flow may lead to increased amounts of melt migrating to the Southeast Greenland margin compared to the Hatton Bank margin. Likewise, as the mantle upwelling is slightly buoyant, there would be a slightly increased component of mantle flow to the west. This could explain the possible observation of asymmetric spreading during the formation of the North Atlantic.

As it is difficult to prescribe the how the melt would segregate on either side of the margin, we have chosen to simply assume that the melt is split evenly between both margins. This assumption allows the prediction of melt production and igneous thickness for the Southeast Greenland margin and a comparison of the melting products of the two possible spreading rates (Figure 15).

If the half spreading rate was $40\,\mathrm{mm\,yr^{-1}}$ during breakup, the two small extension phases prior to rifting have a large impact on the thinning, melt production and resultant igneous crustal thickness (Figure 15). The predicted igneous thickness off the Southeast Greenland margin is close to 17 km. This is in agreement with the 18 km observed in the Sigma III wide angle survey [*Hopper et al.*, 2003; *Holbrook et al.*, 2001]. If the half

spreading rate was $20\,\mathrm{mm\,yr^{-1}}$ during breakup, our model finds that even with a 200 °C hot layer, we cannot recreate the observed igneous thicknesses (Figure 15).

Melt compositions predicted by both models broadly matches the primary melt compositions from ODP sites 917 and 990 (Figure 15). As we are using the *Niu* [1997] melt composition parametrisation, we expect the MgO and FeO composition to be underestimated (see *Armitage et al.*, 2008). However from the more compatible elements, such as TiO_2 and Na_2O, the depletion modelled for both spreading rate models matches reasonably well with the observations. Therefore, despite the predicted 5 % difference in mean melt fraction between models, we do not predict an observable difference in the melt composition that can be differentiated from two cores at similar locations. We would require a time series of primary melt compositions to make such a distinction.

Our model implicitly includes the possible additional effects of small-scale convection [*Nielsen and Hopper*, 2004], and has a thermal anomaly that is similar to the estimated characteristics of the thermal plume that is commonly invoked to explain the North Atlantic Igneous Province [*White and McKenzie*, 1989; *Holbrook et al.*, 2001]. Yet unless there is asymmetric spreading at this margin we cannot reproduce the observed igneous thickness. An alternative interpretation is that the observed igneous crustal thickness is slightly exaggerated at the Southeast Greenland margin because the contribution that is attributed to underplate may be over estimated [*White and Smith*, 2008]. If so then seismic observations at the Southeast Greenland margin may be explained by extension at only slightly elevated half spreading rates during in breakup.

5. Conclusions

1. Simple extension of the lithosphere above a finite reservoir thermal anomaly, such as has been suggested beneath the Southeast Greenland and Hatton Bank margins, will

not produce melt in excess of that expected at steady state without the thermal anomaly. It is only when the lithosphere is thinned prior to rifting, in combination with a thermal anomaly, that excess breakup magmatism is generated.

2. The effect of thinning that resulted in the Hatton-Rockall Trough and a possible pre-rift basin off Greenland, in combination with a thermal anomaly of 200 °C, can reproduce the observed igneous thickness and melt compositions off Southeast Greenland. However, if the margin was symmetric and opened at a slower half spreading of $20\,\mathrm{mm\,yr^{-1}}$, then we under-predict the observed igneous thickness.

3. Time is a key factor. The thermal anomaly is required to be a transient feature and likewise the prior thinning of the lithosphere only lasts for a certain period of time, as the lithosphere cools. The importance of the thickness of the lithosphere at the time of rifting has been shown. It is clear that simple assumptions for the amount of extension cannot be made, as the rift is sensitive to the amount of pre-thinned extension undergone, and how far the rift is from that pre-thinned region. Likewise, the pre-thinning event remains of importance to rift development for many years (~ 30 Myrs). Therefore rifts cannot be considered in isolation, the transient effects of prior events must also be accounted for.

4. Given these considerations, the high volumes of material emplaced during the opening of the North Atlantic requires a pre-thinning event. Without thinned lithosphere prior to breakup there would be no excess melt production due to the thickness of the lithosphere dampening any upwelling. We therefore argue that, no matter the thermal state of the lithosphere, for the emplacement of large amounts of melt at slow rates of extension, the lithosphere must have undergone some extension prior to breakup.

Acknowledgments. We are grateful for constructive conversations with John Maclennan and Rex Taylor. The manuscript benefited from very constructive reviews by Ritske

Huismans and an anonymous reviewer. This project was supported by the NERC Oceans Margins LINK thematic program through a studentship for John Armitage.

References

Armitage, J. J., T. J. Henstock, T. A. Minshull, and J. R. Hopper, Modelling the composition of melts formed during continental break-up of the North Atlantic, *Earth Planetary Science Letters*, *269*, 248–258, 2008, doi: 10.1016/j.epsl.2008.02.024.

Barton, P. F., and R. S. White, Crustal structure of the Edoras Bank margin and mantle thermal anomalies beneath the North Atlantic, *Journal of Geophysical Research*, *103*, 3109–3129, 1997.

Bassi, G., C. E. Keen, and P. Potter, Contrasting styles of rifting - models and examples from the eastern Canadian margin, *Tectonics*, *12*, 639–655, 1993.

Boutilier, R. P., and C. E. Keen, Small-scale convection and divergent plate boundaries, *Journal of Geophysical Research*, *104*, 7389–7403, 1999.

Bown, J. W., and R. S. White, Effect of finite extension rate on melt generation at rifted continental margins, *Journal of Geophysical Research*, *100*, 18,011–18,029, 1995.

Cooper, C. M., A. Lenardic, and L. Moresi, The thermal structure of stable continental lithosphere within a dynamic mantle, *Earth and Planetary Science Letters*, *222*, 807–817, 2004, doi: 10.1016/j.epsl.2004.04.008.

Corti, G., and P. Manetti, Asymmetric rifts due to asymmetric Mohos: an experimental approach, *Earth and Planetary Science Letters*, *245*, 315–329, 2006.

Corti, G., J. van Wijk, M. Bonini, D. Sokoutis, S. Cloetingh, F. Innocenti, and P. Manetti, Transition from continental break-up to punctiform seafloor spreading: How fast, asymmetric and magnetic, *Geophysical Research Letters*, *30*, 1604, 2003, doi: 10.1029/2003GL017374.

Dean, S. M., B. J. Murton, T. A. Minshull, T. A. Henstock, and R. S. White, An integrated kinematic and geochemical model to determine lithospheric extension and mantle temperatures from syn-rift volcanic compositions, *Earth and Planetary Science Letters*, 2008, doi: 10.1016/j.epsl.2008.11.012.

Doré, A. G., E. R. Lundin, L. N. Jensen, O. Birkeland, P. E. Eliassen, and C. Filcher, Principal tectonic events in the evolution of the Northwest European Atlantic margin, in *Petroleum Geology of Northwest Europe: Proceedings of the 5th Conference*, edited by A. J. Fleet and S. A. R. Boldy, pp. 41–61, Geological Society, London, 1999.

Edwards, J. W. F., Development of the Hatton-Rockall Basin, North-East Atlantic Ocean, *Marine and Petroleum Geology*, *19*, 193–205, 2002.

England, P., Constraints on extension of continental lithosphere, *Journal of Geophysical Research*, *88*, 1145–1152, 1983.

Hitchen, K., The geology of the UK Hatton-Rockall margin, *Marine and Petroleum Geology*, *21*, 993–1012, 2004.

Holbrook, W. S., et al., Mantle thermal structure and active upwelling during continental breakup in the north Atlantic, *Earth and Planetary Science Letters*, *190*, 251–266, 2001.

Hopper, J. R., T. Dahl-Jensen, W. S. Holbrook, H. C. Larsen, D. Lizarradle, J. Korenaga, G. M. Kent, and P. B. Kelemen, Structure of the SE Greenland margin from seismic reflection and refraction data: Implications for nascent spreading centre subsidence and asymmetric crustal accretion during North Atlantic opening, *Journal of Geophysical Research*, *108*, doi: 10.1029/2002JB001,996, 2003.

Houseman, G., and P. England, A dynamical model for lithosphere extension and sedimentary basin formation, *Journal of Geophysical Research*, *91*, 719–729, 1986.

Ito, G., J. Lin, and C. W. Gable, Dynamics of mantle flow and melting at ridge-centred hotspot: Iceland and the Mid-Atlantic Ridge, *Earth and Planetary Science Letters*, *144*, 53–74, 1996.

Jurine, D., C. Jaupart, G. Brandeis, and P. J. Tackley, Penetration of mantle plumes through depleted lithosphere, *Journal of Geophysical Research*, *110*, 2005, doi: 10.1029/2005JB003751.

Keen, C. E., and R. B. Boutilier, Interaction of rifting and hot horizontal plume sheets at volcanic margins, *Journal of Geophysical Research*, *105*, 13,375–13,387, 2000.

King, S. D., and D. L. Anderson, An alternative mechanism of flood basalt formation, *Earth and Planetary Science Letters*, *160*, 289–296, 1998.

Larsen, B., A marine geophysical survey of the East Greenland continental shelf between latitudes 60° and 70°N - project DANA, *The Geological Survey of Greenland Report*, *100*, 94–98, 1980.

Larsen, H., and A. Saunders, Tectonism and volcanism at the southeast Greenland rifted margin: A record of plume impact and later continental rupture, *Proceedings of the Ocean Drilling Program, Scientific Results*, *152*, 503–533, 1998.

Larsen, H. C., H. C. Saunders, P. D. Clift, and *et al* (Eds.), *Proceedings of the Ocean Drilling Program, Scientific Results, 152*, Ocean Drilling Program, College Station, TX, 1994.

Larsen, L. M., J. G. Fitton, and M. S. Fram, Volcanic rocks of the southeast Greenland margin in comparison with other parts of the north Atlanic tertiary igneous province, *Proceedings of the Ocean Drilling Program, Scientific Results*, *152*, 315–330, 1998.

Larsen, L. M., J. G. Fitton, and A. D. Saunders, Composition of volcanic rocks from the Southeast Greenland margin, leg 163: major and trace element geochemistry, *Proceed-*

ings of the Ocean Drilling Program, Scientific Results, *163*, 63–75, 1999.

McKenzie, D., J. Jackson, and K. Priestley, Thermal structure of oceanic and continental lithosphere, *Earth and Planetary Science Letters*, *233*, 337–349, 2005.

McKenzie, D. P., Some remarks on the development of sedimentary basins, *Earth and Planetary Science Letters*, *40*, 25–32, 1978.

McKenzie, D. P., and M. J. Bickle, The volume and composition of melt generated by extension of the lithosphere, *Journal of Petrology*, *29*, 625–679, 1988.

Meyer, R., J. van Wijk, and L. Gernignon, The North Atlantic igneous province: A review of models for its formation, in *Special Paper 430: Plates, Plumes and Planetary Processes*, edited by G. R. Foulger and D. M. Jury, pp. 525–552, The Geological Society of America, 2007.

Mittelsteadt, E., G. Ito, and M. D. Behn, Mid-ocean ridge jumps associated with hotspot magmatism, *Earth and Planetary Science Letters*, *266*, 256–270, 2008, doi: 10.1016/j.epsl.2007.10.055.

Mjelde, R., T. Raum, B. Myhren, H. Shimamura, Y. Murai, T. Takanami, R. Karpz, and U. Naess, Continent-ocean transition on the Vøring Plateau, NE Atlantic, derived from densely spaced ocean bottom seismometer data, *Journal of Geophysical Research*, *110*, 2005, doi:10.1029/2004JB003026.

Moresi, L., S. Zhong, and M. Gurnis, The accuracy of finite element solutions of Stokes' flow with strongly varying viscosity, *Physics of the Earth and Planetary Interiors*, *97*, 83–94, 1996.

Nielsen, T. K., and J. R. Hopper, Formation of volcanic rifted margins: are temperature anomalies required?, *Geophysical Research Letters*, *29*, doi: 10.1029/2002GL015,681, 2002.

Nielsen, T. K., and J. R. Hopper, From rift to drift: mantle melting during continental breakup, *Geochemistry Geophysics Geosystems*, *5*, doi: 10.1029/2003GC000,662, 2004.

Niu, Y., Mantle melting and melt extraction processes beneath ocean ridges: Evidence from abyssal peridotites, *Journal of Petrology*, *38*, 1047–1074, 1997.

Peate, I. U., M. Larsen, and C. E. Lesher, The transition from sedimentation to flood volcanism in the Kangerlussuaq Basin, East Greenland: basaltic pyroclastic volcanism during initial Palaeogene continental break-up, *Journal of the Geological Society, London*, *160*, 759–772, 2003.

Phipps Morgan, J., Thermodynamics of pressure release melting of a veined plum pudding mantle, *Geochemistry Geophysics Geosystems*, *2*, 2001, doi: 10.1029/2000GC000049.

Plank, T., M. Spiegelman, C. H. Langmuir, and D. W. Forsyth, The meaning of 'mean F': Clarifying the mean extent of melting at ocean ridges, *Journal of Geophysical Research*, *100*, 15,045–15,052, 1995.

Reston, T., Extension discrepancy at North Atlantic nonvolcanic rifted margins: Depth-dependent stretching or unrecognized faulting?, *Geology*, *35*, 364–370, 2007, doi: 10.1130/G23213A.1.

Scott, D. R., Small-scale convection and mantle melting beneath mid-ocean ridges, in *Mantle flow and melt generation at mid-ocean ridges*, edited by J. Phipps Morgan, D. K. Blackman, and J. M. Sinton, vol. Geophysical Monograph 71, pp. 327–352, American Geophysical Union, 1992.

Shannon, P. M., The development of Irish offshore sedimentary basins, *Journal of the Geological Society, London*, *148*, 181–189, 1991.

Shannon, P. M., J. G. Moore, A. W. B. Jacob, and J. Makris, Cretaceous and Tertiary basin development west of Ireland, in *Petroleum Geology of Northwest Europe: Proceed-*

ings of the 4th Conference, edited by J. R. Parker, pp. 1057–1066, Geological Society, London, 1993.

Simon, K., R. S. Huismans, and C. Beaumont, Dynamical modelling of lithospheric extension and small-scale convection: implications for magmatism during the formation of volcanic rifted margins, *Geophysical Journal International*, *176*, 327–350, 2009, doi: 10.111/j.1365-246X.2008.03891.x.

Sleep, N. H., Lateral flow of hot plume material ponded at sublithospheric depths, *Journal of Geophysical Research*, *101*, 28,065–28,083, 1996.

Sleep, N. H., Ege-modulated stagnant-lid convection and volcanic passive margins, *Geochemistry Geophysics Geosystems*, *8*, 2007, doi: 10.1029/2007GC001672.

Smallwood, J. R., and R. S. White, Ridge-plume interaction in the North Atlantic and its influence on continental breakup and seafloor spreading, in *The North Atlantic igneous province: Stratigraphy, tectonic, volcanic and magmatic processes*, edited by D. W. Jolley and B. R. Bell, pp. 15–37, The Geological Society of London, 2002.

Smith, L. K., R. S. White, N. J. Kusznir, and iSIMM Team, Structure of the Hatton Basin and adjacent continental margin, in *Petroleum Geology: North-West Europe and Global Perspectives - Proceedings of the 6th Petroleum Geology Conference*, edited by A. G. Doré and B. A. Vining, pp. 947–956, Geological Society, London, 2005.

Smythe, D. K., Rockall Trough - Cretaceous or late Palaeozoic, *Scottish Journal of Geology*, *25*, 5–43, 1989.

Storey, M., R. A. Duncan, and C. C. Swisher III, Paleocene-Eocene thermal maximum and opening of the Northeast Atlantic, *Science*, *316*, 587–589, 2007, doi: 10.1126/science.1135274.

Thy, P., C. E. Lesher, and M. S. Fram, Low pressure experimental constraints on the evolution of basaltic lavas from site 917, southeast Greenland continental margin, *Proceedings of the Ocean Drilling Program, Scientific Results*, *152*, 359–372, 1998.

van Wijk, J. W., and S. A. P. L. Cloetingh, Basin migration caused by slow lithospheric extension, *Earth and Planetary Science Letters*, *198*, 275–288, 2002.

Voss, M., and W. Jokat, Continent-ocean transition and voluminous magmatic underplating derived from P-wave velocity modelling of the East Greenland continental margin, *Geophysics Journal International*, *170*, 580–605, 2007.

White, R. S., and D. P. McKenzie, Magmatism at rift zones: the generation of volcanic continental margins and flood basalts, *Journal of Geophysical Research*, *94*, 7685–7729, 1989.

White, R. S., and L. K. Smith, Crustal structure of the Hatton and the conjugate east Greenland rifted volcanic continental margins, NE Atlantic, *Journal of Geophysical Research*, 2008.

White, R. S., L. K. Smith, A. W. Roberts, P. A. F. Christie, N. J. Kusznir, and the rest of the iSIMM Team, Lower-crustal intrusion on the North Atlantic continental margin, *Nature*, *452*, 460–465, 2008, doi: 10.1038/nature06687.

Table 1. Model parameters and assumed values

Variable	Meaning and Units	Value
c_p	specific heat capacity, $\mathrm{J\,kg^{-1}\,K^{-1}}$	1200
C	instantaneous major element melt composition	
$\overline{C}$	mean major element melt composition	
g	acceleration of gravity, $\mathrm{m\,s^{-2}}$	9.8
E	activation energy, $\mathrm{J\,mol^{-1}}$	530×10^3
F	melt fraction	
$\overline{F}$	mean melt fraction	
L	Latent heat upon melting	$\mathrm{J\,mol^{-1}}$
$\dot{m}$	dimensionless melt production rate	
M	mass of the melt phase	kg
M_0	initial total mass	kg
n	stress exponent	3
p	pressure, Pa	
R	gas constant, $\mathrm{J\,K^{-1}\,mol^{-1}}$	8.314
T	mantle temperature, K	
T_s	wet or dry solidus temperature, K	
T_{s0}	dry solidus surface temperature, K	1373
u	mantle creep, $\mathrm{m\,s^{-1}}$	
V	activation volume, $\mathrm{m^3\,mol^{-1}}$	5×10^{-6}
X	concentration of perfectly compatible trace element	
$\dot{\epsilon}$	strain rate, $\mathrm{s^{-1}}$	
γ	coefficient of melt density reduction	0.16
κ	thermal diffusivity, $\mathrm{m^2\,s^{-1}}$	10^{-6}
η	viscosity, Pa s	
ϕ	retained melt (porosity)	
ρ_m	mantle reference density, $\mathrm{kg\,m^{-3}}$	3340
ρ_l	melt density, $\mathrm{kg\,m^{-3}}$	2800
τ	deviatoric stress, Pa	
χ_{H_2O}	viscosity increase factor due to dehydration	$0 - 100$
χ_m	viscosity reduction factor due to interstitial melt	

Figure 1. Diagram of model space showing the thermally and rheologically defined 125 km thick lithosphere with the option of imposing pre-thinning at the centre of extension as an initial condition. Finally there is a thermal anomaly of variable thickness below. Boundary conditions are of free slip on all sides except the top surface, where we imposed divergent spreading at a constant half spreading rate. Temperature is held fixed at 0 °C at the top surface and at 1325 °C at the base. The temperature gradient across the side boundaries is held fixed at zero.

Table 2. Series of extension phases leading up to the opening of the Southeast Greenland and Hatton Bank margin

Age	Phase of Extension	Event
91 Ma – 80 Ma	1	Extension of a Hatton-Rockall like basin to a stretching factor of 2, at a half spreading rate of $5\,\mathrm{mm\,yr^{-1}}$.
80 Ma – 62 Ma		No extension
62 Ma – 61 Ma	2	Extension of the pre-rift basin, after a shift in the centre of extension of 100 km to the west to a stretching factor of 1.1, at a half spreading rate of $10\,\mathrm{mm\,yr^{-1}}$.
61 Ma – 56 Ma	3	Extension and rifting of the Southeast Greenland and conjugate Hatton Bank margins above a 200 °C thermal anomaly, at a half spreading rate of either 20 or $40\,\mathrm{mm\,yr^{-1}}$.
56 Ma – present		Continued rifting at $10\,\mathrm{mm\,yr^{-1}}$.

Figure 2. Igneous crustal thickness and selected major element composition of melt for the two initial conditions: *Case 1*, where the lithosphere is a flat layer with no thinned regions and no thermal anomaly beneath, and *Case 2*, where a 50 km thick 200 °C thermal anomaly exists beneath the flat lithosphere. Half spreading rate is increased from 10 to $50\,\mathrm{mm\,yr^{-1}}$.

Figure 3. A comparison of *Case 2* with *Case 3*, where the thickness of the 200 °C thermal anomaly is increased from 50 km to 100 km. (a) in these four panels are on the left, plots of temperature where the 1375 °C isotherm has been contoured to help define the thermal anomaly, and streamlines of flow in the mantle; on the right is viscosity and contours of melt fraction F at 0, 0.1 and 0.2. These properties are plotted for a 200 by 200 km region at the centre of extension. We plot the model conditions at 17.6 Myrs, as this is the peak in igneous thickness. On the right are comparisons of: (b) igneous crustal thickness, h_c; (c) ratio of the average upwelling velocity within the melting region to the half spreading rate; (d) mean mantle temperature within the melting region; and (e) mean melt fraction within the melt region, $\overline{F}$.

Figure 4. Igneous crustal thickness and selected major element composition of melt for the two initial conditions: *Case 4*, where the lithosphere is pre-thinned as an initial condition, with no thinned regions and no thermal anomaly beneath, and *Case 5*, where a 50 km thick 200 °C thermal anomaly exists beneath the pre-thinned lithosphere. Half spreading rate is increased from 10 to 50 mm yr^{-1}.

Figure 5. Effect of a pre-thinned region as an initial condition without the presence of a thermal anomaly (*case 1* and *4*): (a) Igneous crustal thickness; (b) ratio of the average upwelling velocity within the melting region against the half spreading rate; (c) mean mantle temperature within the melt region; and (d) mean melt fraction within the melt region.

Figure 6. Comparison of the effect of a pre-thinned region as an initial condition in the presence of a 50 km 200 °C thermal anomaly (*case 2* and *5*). (a) in these four panels are plots of temperature and flow of the mantle; and viscosity and contours of 0, 2 and 10 % melt production. These properties are plotted for a 200 by 200 km region at the centre of extension. The ages chosen are that of peak melt generation for each model. On the right are comparisons of: (b) igneous crustal thickness; (c) ratio of the average upwelling velocity within the melting region to the half spreading rate; (d) mean mantle temperature within the melting region; and (e) mean melt fraction within the melt region.

Figure 7. Diagram of a hypothetical situation where there is a previous region of extension offset from the position of the new rift. I extend the lithosphere at $5\,\mathrm{mm\,yr^{-1}}$ for a set period of time to gain the appropriate stretching factor. The rifting is offset to the left by shifting the kinematic boundary condition of spreading.

Figure 8. Model results for two stage rifting where hot layer is emplaced as a uniform thickness layer at fixed depth: an initial period of extension at a half spreading rate of $5\,\mathrm{mm\,yr^{-1}}$ that lasts 17 Myrs. At this point the lithosphere is extended by a factor of 5. The centre of extension shifts to the east by 44 km, and a 50 km thick 200 °C thermal anomaly is emplaced beneath the lithosphere. Extension continues thereafter at a half spreading rate of $10\,\mathrm{mm\,yr^{-1}}$. Plotted from left to right: are temperature with the 1425 °C isotherm contoured; melt fraction and stream lines of flow; and mantle viscosity.

Figure 9. Comparisons of the peak igneous thickness during rifting: (a) Initial phase of extension at $5\,\mathrm{mm\,yr^{-1}}$ followed by the second phase of extension at a half spreading rate of $10\,\mathrm{mm\,yr^{-1}}$ above a 50 km thick 200 °C thermal anomaly. (b) Initial phase of extension at different half spreading rates, 5 to $50\,\mathrm{mm\,yr^{-1}}$, followed by the second phase of extension at a half spreading rate of $10\,\mathrm{mm\,yr^{-1}}$ above a 50 km thick 200 °C thermal anomaly, which initiates 88 km away from the initial period of extension. The grey circles mark the model results from which the contours have been interpolated.

Figure 10. Model results for two stage rifting where hot layer is emplaced as uniform thickness layer that follows the lithospheric boundary, referred to as the *drape* model: an initial period of extension at a half spreading rate of $5\,\mathrm{mm\,yr^{-1}}$ that lasts 17 Myrs. At this point the lithosphere is extended by a factor of 5. The centre of extension shifts to the east by 44 km, and a 50 km thick 200 °C thermal anomaly is draped beneath the lithosphere. Extension continues thereafter at a half spreading rate of $10\,\mathrm{mm\,yr^{-1}}$. Plotted from left to right: are temperature with the 1425 °C isotherm contoured; melt fraction and stream lines of flow; and mantle viscosity.

Figure 11. Model results for two stage rifting where hot material ponds into lithospheric thin spots: an initial period of extension at a half spreading rate of $5\,\mathrm{mm\,yr^{-1}}$ that lasts 17 Myrs. At this point the lithosphere is extended by a factor of 5. The centre of extension shifts to the east by 44 km, and a 200 °C thermal anomaly is ponds beneath the lithosphere such that the base of the thermal anomaly is at 175 km depth. Extension continues thereafter at a half spreading rate of $10\,\mathrm{mm\,yr^{-1}}$. Plotted from left to right: are temperature with the 1425 °C isotherm contoured; melt fraction and stream lines of flow; and mantle viscosity.

Figure 12. A comparison of the evolution of three different thermal anomaly emplacement styles, (a) Igneous crustal thickness; (b) ratio of the average upwelling velocity within the melting region against the half spreading rate; (c) mean mantle temperature within the melt region; and (d) mean melt fraction within the melt region. Compared are: *Uniform*, a uniformly 50 km thick thermal anomaly at 125 km depth; *Drape*, a 50 km thick thermal anomaly that is draped beneath the thinned lithosphere; and *Ponded*, a thermal anomaly that extends to a depth of 175 km and has ponded beneath the thinned region of lithosphere.

Figure 13. Reconstruction of the North Atlantic to using GPlates and a cross section of the lithosphere just prior to breakup during the Paleocene to Early Eocene ($\sim 60\,Ma$). Shown diagrammatically are; in light blue and lilac, regions of extension during the Mid-Cretaceous; in dark blue and green, regions of extension that occurred during the Late Cretaceous to Early-Eocene including the Hatton-Rockall (HR) Basin [*Larsen*, 1980; *Doré et al.*, 1999]. Also shown diagrammatically is the subsequent centre of extension during rifting. The cross section A to A' shows the possible sublithospheric topography as a consequence of the prior extensional events. The thermal anomaly, shown in red, would be expected to advect into the pre-thinned region due to the earlier extensional events.

Figure 14. Model results for the North Atlantic. From bottom to top: 61 Ma just prior to the arrival of the sublithospheric hot layer, 56 Ma once the fast period of extension at a half spreading rate of $20\,\mathrm{mm\,yr^{-1}}$ has ceased, and the following panels show the subsequent evolution of the margin. The panels show the same properties as Figure 8.

Figure 15. Comparison of simulated multiphase rift evolutions for the Southeast Greenland margin. Rifting at a half spreading rate of $10\,\mathrm{mm\,yr^{-1}}$ follows after a two initial periods of extension. The solid line is for a model with a $200\,^{\circ}\mathrm{C}$ thermal anomaly and an initial pulse of faster extension at $20\,\mathrm{mm\,yr^{-1}}$. The dashed line is for an initial pulse of faster extension at $40\,\mathrm{mm\,yr^{-1}}$. Plotted are the igneous crustal thickness, mean melt fraction and major element melt composition. These are compared to the observed igneous crustal thickness from the Sigma III survey [*Holbrook et al.*, 2001] and primary compositions estimated from ODP sites 990 and 917 [*Larsen et al.*, 1998; *Thy et al.*, 1998; *Larsen et al.*, 1999].

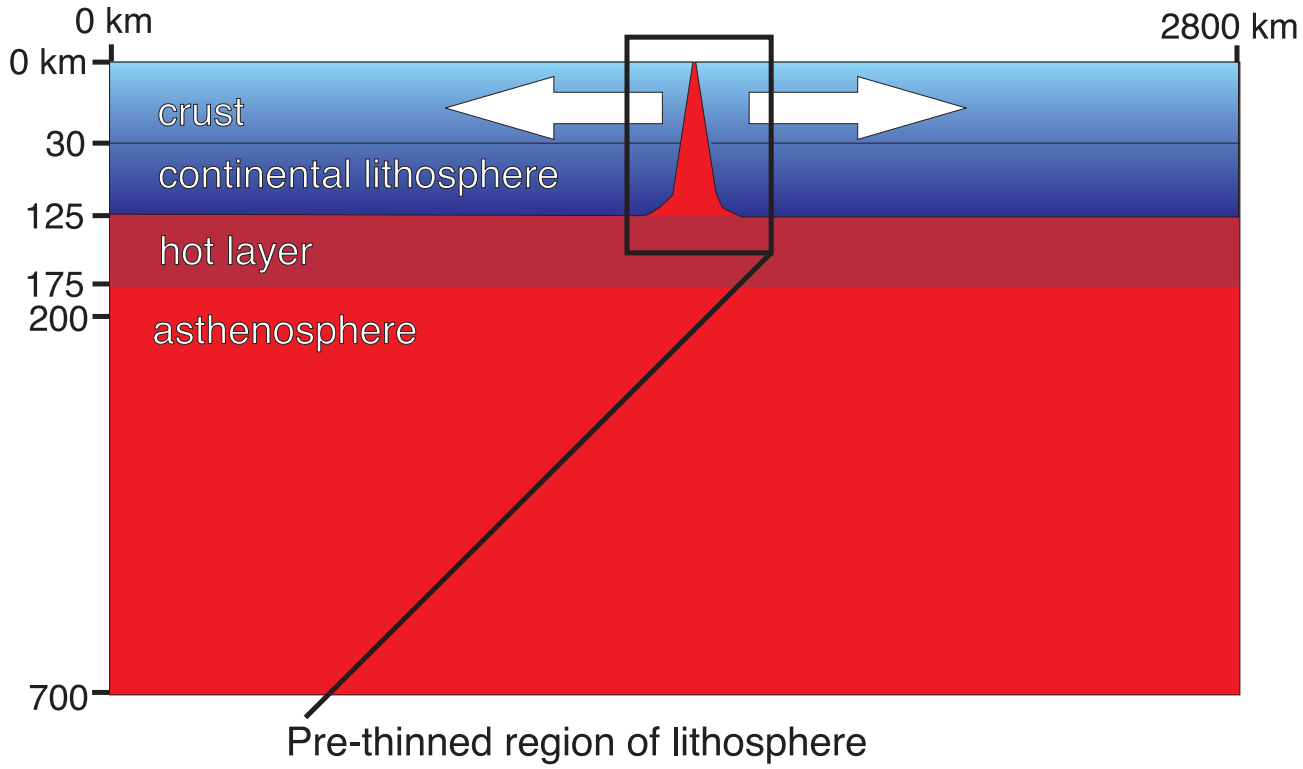
0 km
2800 km
0 km
crust
30
continental lithosphere
125
hot layer
175
200
asthenosphere
700
Pre-thinned region of lithosphere

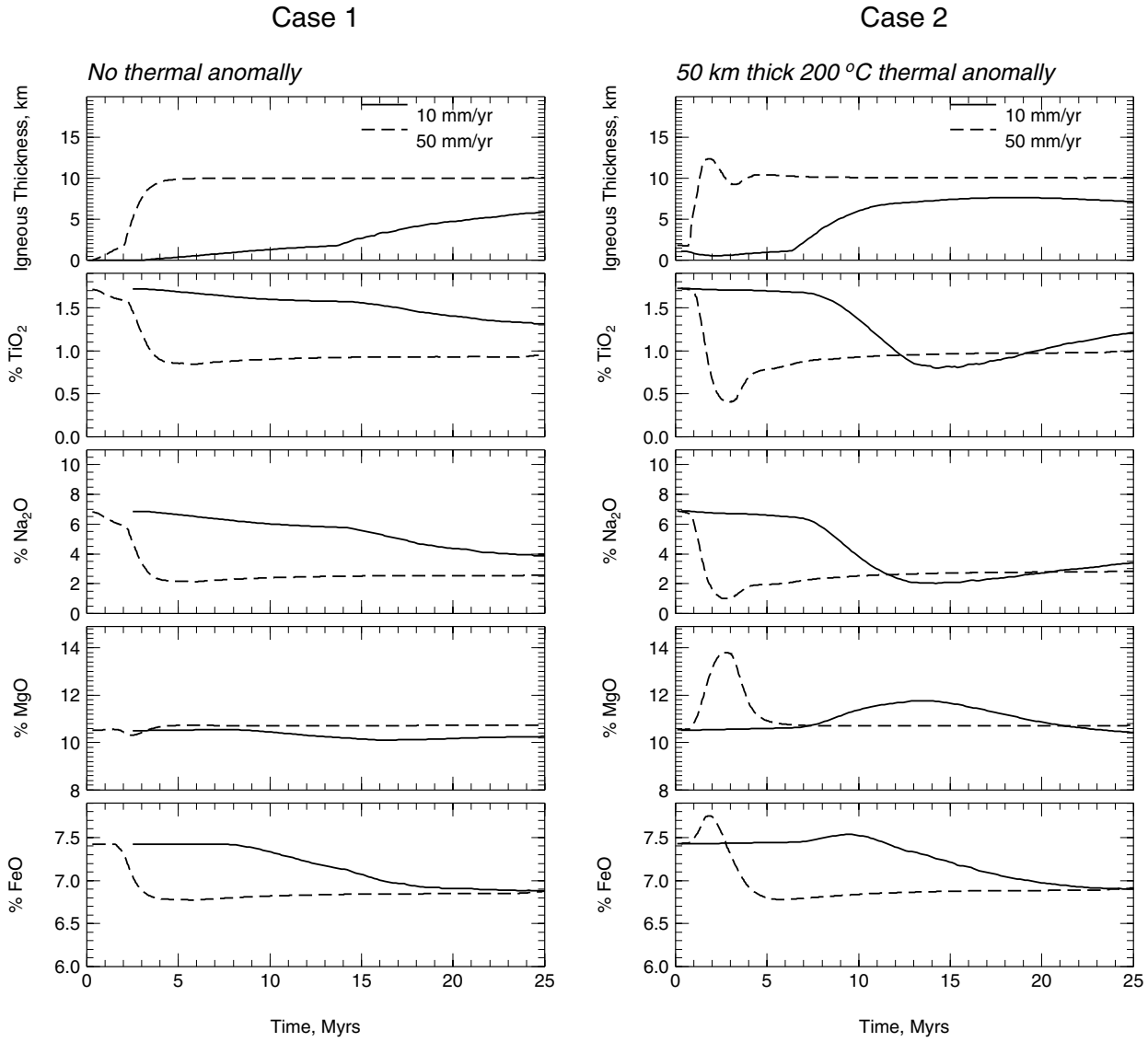
Case 1
No thermal anomally
Case 2
50 km thick 200 °C thermal anomally
10 mm/yr
50 mm/yr
Igneous Thickness, km
% TiO2
% Na2O
% MgO
% FeO
Time, Myrs

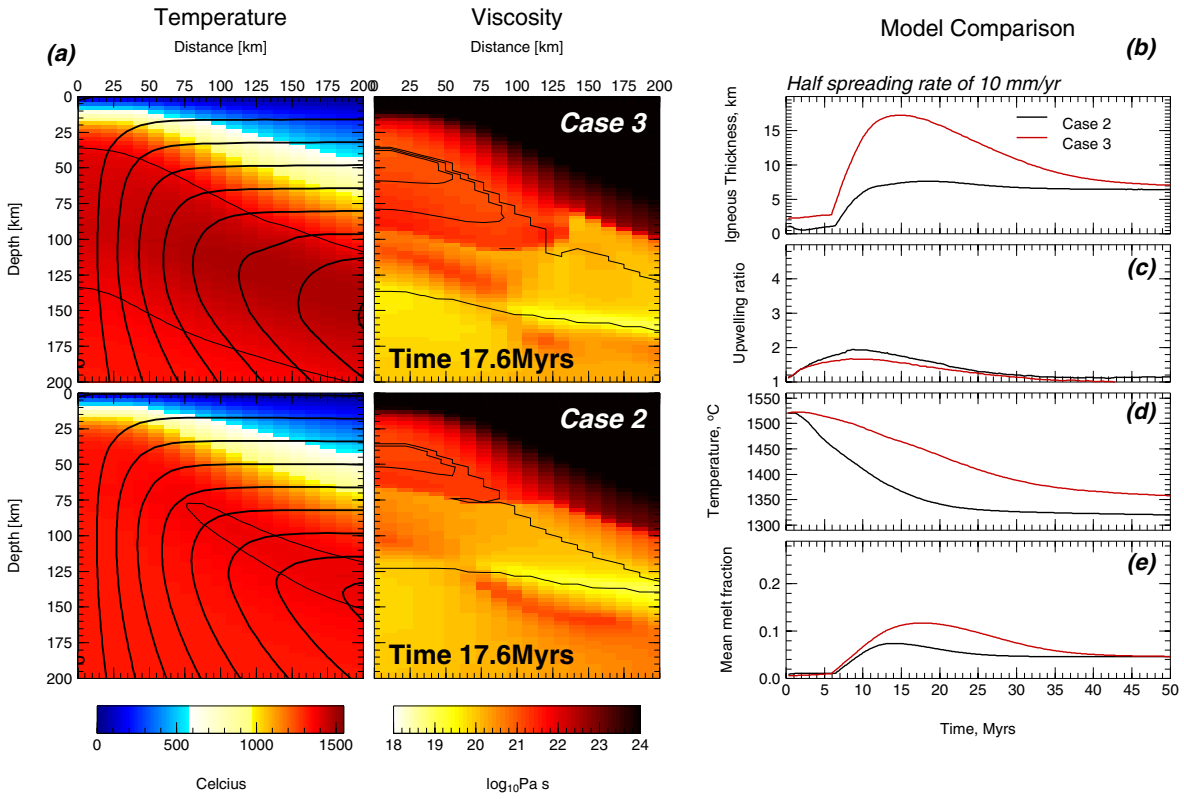
Temperature
Viscosity
(a)
Distance [km]
Distance [km]
Case 3
Time 17.6Myrs
Case 2
Time 17.6Myrs
Depth [km]
Depth [km]
Celcius
log10Pa s
Model Comparison
(b)
Half spreading rate of 10 mm/yr
Case 2
Case 3
Igneous Thickness, km
(c)
Upwelling ratio
(d)
Temperature, °C
(e)
Mean melt fraction
Time, Myrs

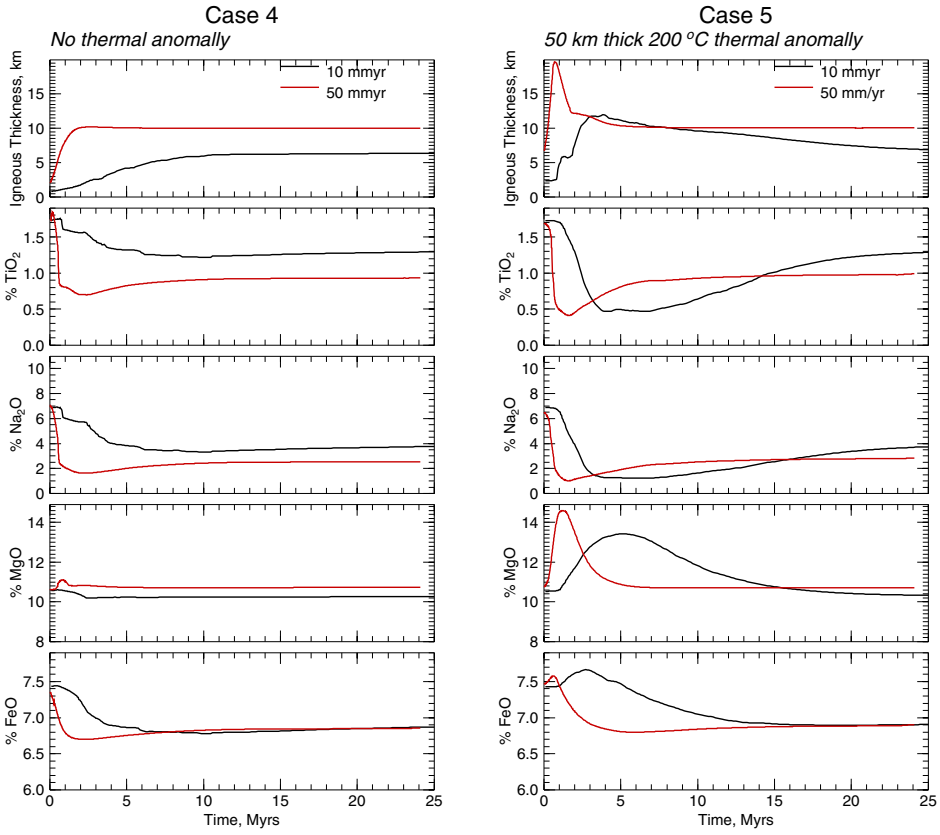
Case 4
No thermal anomally
Case 5
50 km thick 200 °C thermal anomally
10 mmyr
50 mmyr
10 mmyr
50 mm/yr
Igneous Thickness, km
% TiO2
% Na2O
% MgO
% FeO
Time, Myrs
Time, Myrs

Case 1 – Case 4

10 mmyr^{-1} half spreading rate

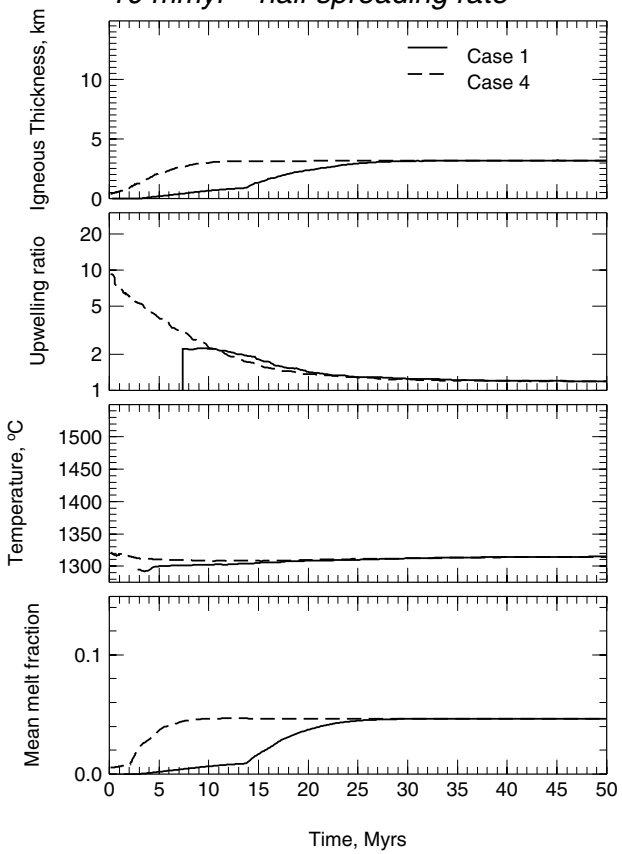

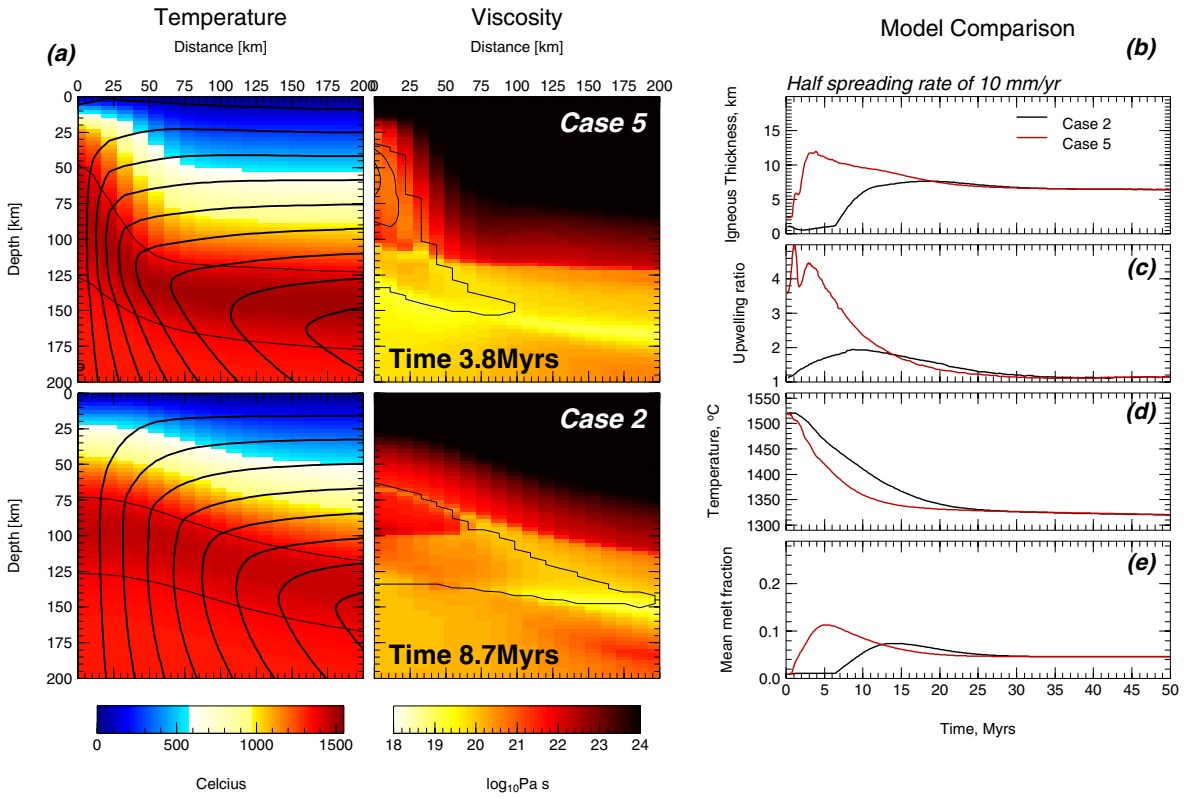
Temperature
Viscosity
(a)
Distance [km]
Distance [km]
Depth [km]
Depth [km]
Case 5
Time 3.8Myrs
Case 2
Time 8.7Myrs
Celcius
log10Pa s
Model Comparison
(b)
Half spreading rate of 10 mm/yr
Case 2
Case 5
Igneous Thickness, km
(c)
Upwelling ratio
(d)
Temperature, °C
(e)
Mean melt fraction
Time, Myrs

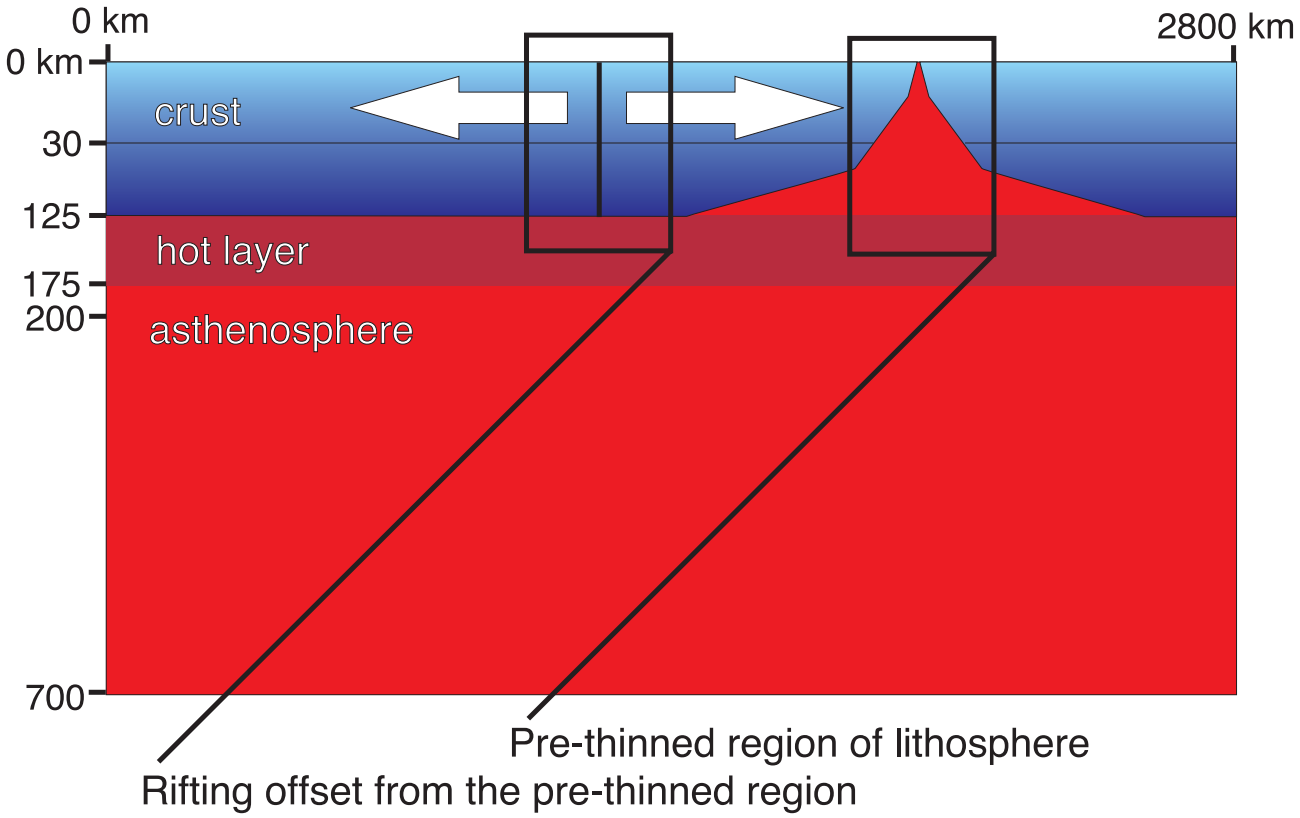
0 km
2800 km
0 km
crust
30
125
hot layer
175
200
asthenosphere
700
Pre-thinned region of lithosphere
Rifting offset from the pre-thinned region

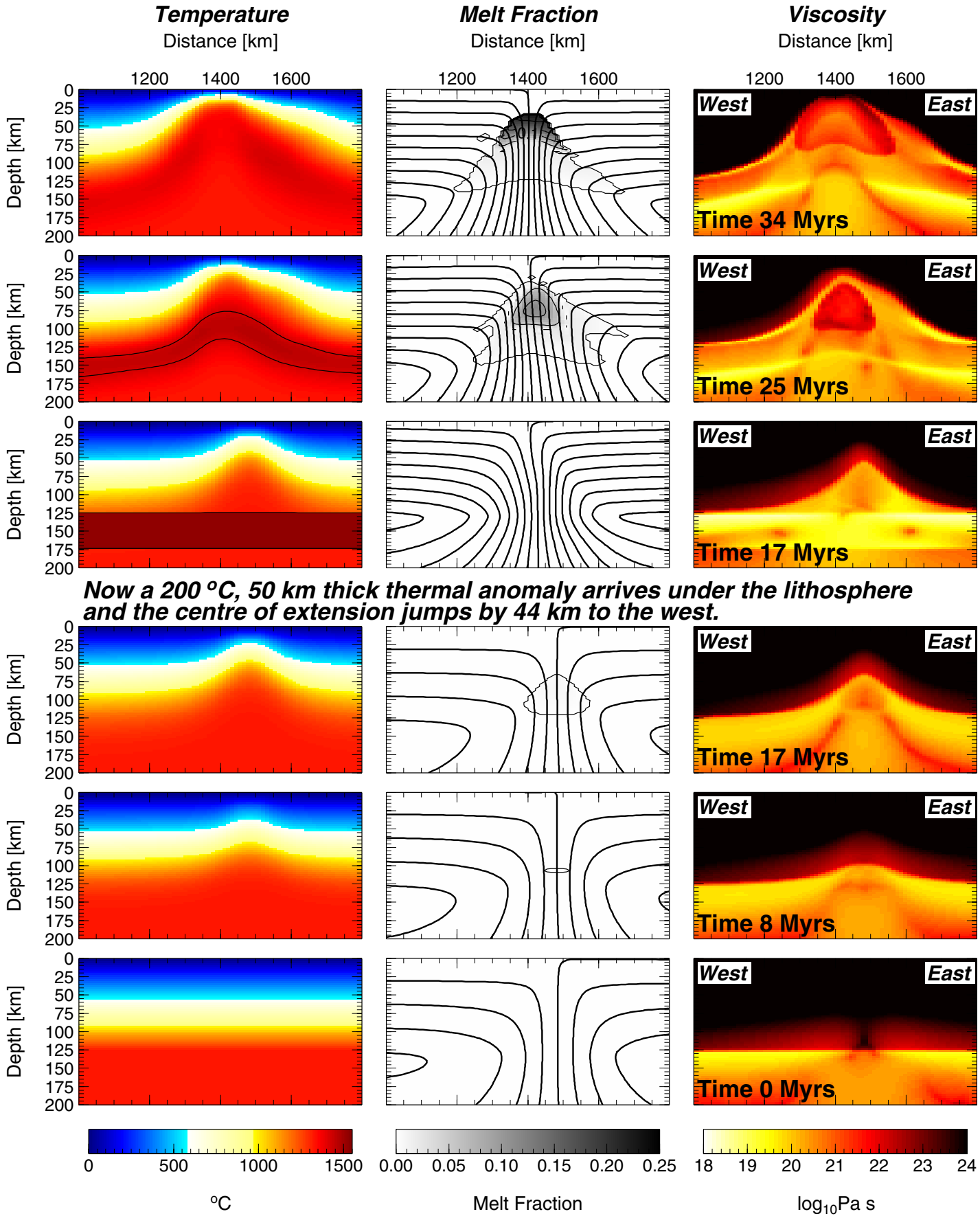
Temperature
Melt Fraction
Viscosity
Distance [km]
1200
1400
1600
Depth [km]
0
25
50
75
100
125
150
175
200
West
East
Time 34 Myrs
Time 25 Myrs
Time 17 Myrs
Now a 200 °C, 50 km thick thermal anomaly arrives under the lithosphere and the centre of extension jumps by 44 km to the west.
Time 17 Myrs
Time 8 Myrs
Time 0 Myrs
0
500
1000
1500
°C
0.00
0.05
0.10
0.15
0.20
0.25
Melt Fraction
18
19
20
21
22
23
24
log10Pa s

(a) ***Effect of distance between two events***

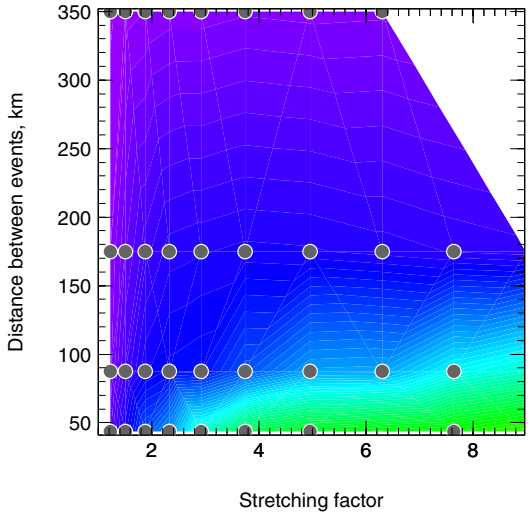

(b) ***Effect of increased extension during initial extension event***

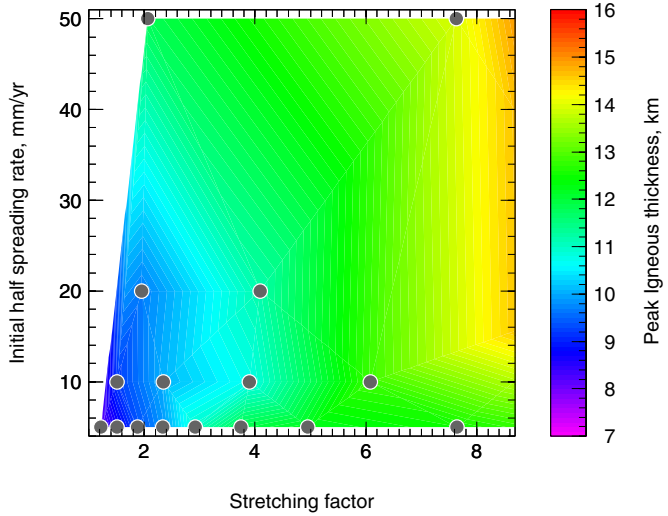

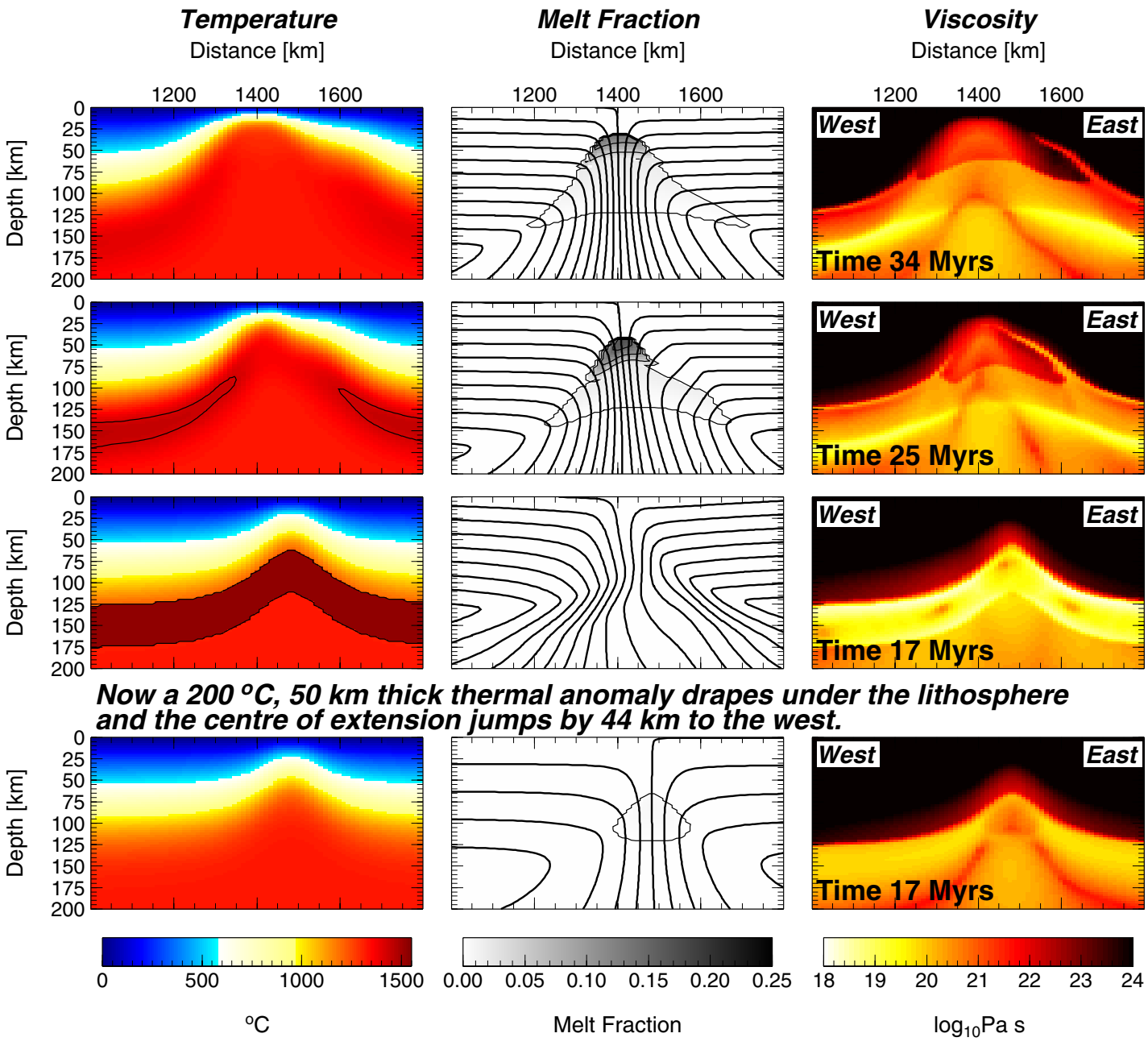
Temperature
Melt Fraction
Viscosity
Distance [km]
1200
1400
1600
Depth [km]
0
25
50
75
100
125
150
175
200
West
East
Time 34 Myrs
Time 25 Myrs
Time 17 Myrs
Now a 200 ºC, 50 km thick thermal anomaly drapes under the lithosphere and the centre of extension jumps by 44 km to the west.
0
500
1000
1500
ºC
0.00
0.05
0.10
0.15
0.20
0.25
Melt Fraction
18
19
20
21
22
23
24
log10Pa s

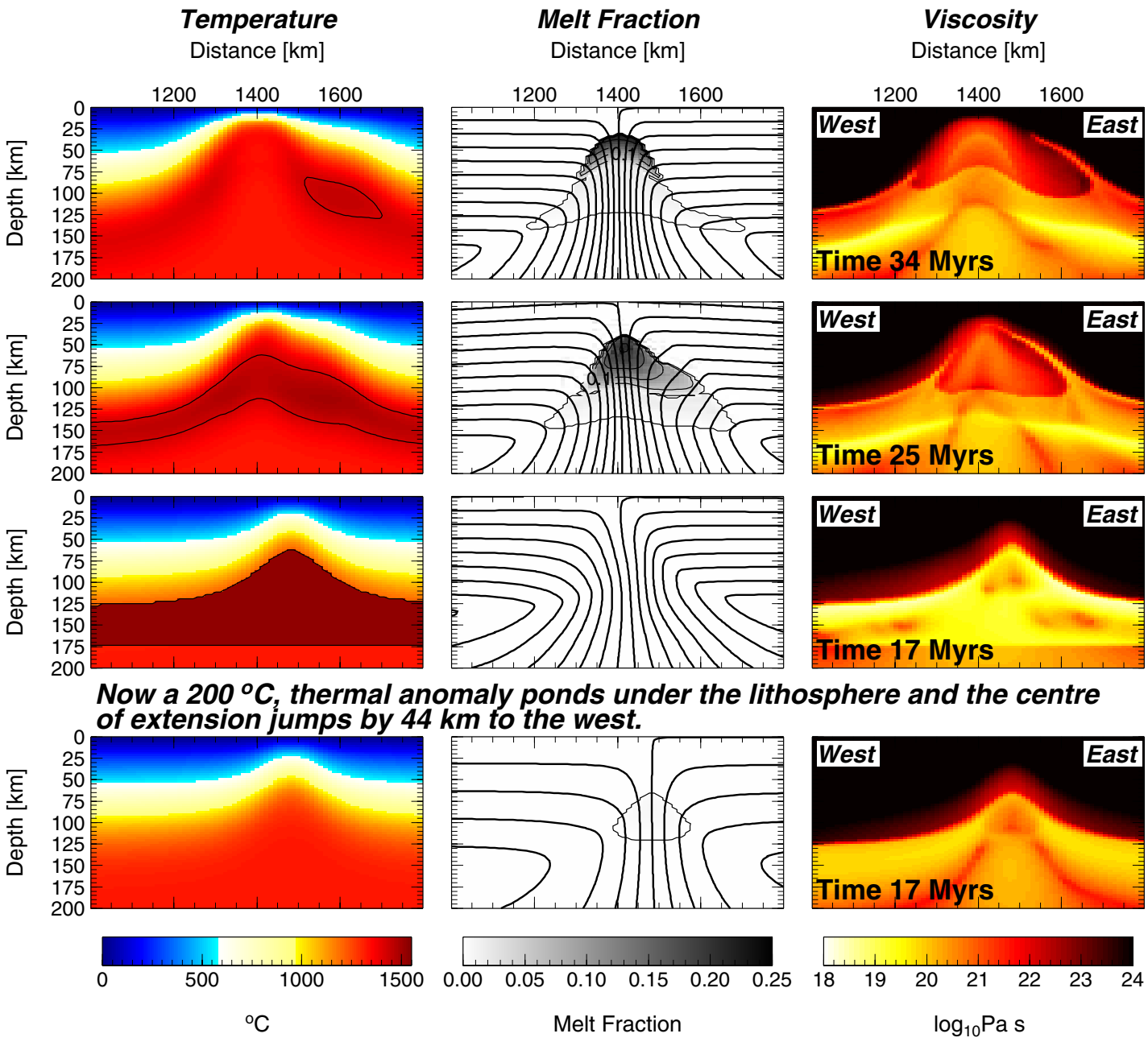
Temperature
Melt Fraction
Viscosity
Distance [km]
1200
1400
1600
Depth [km]
0
25
50
75
100
125
150
175
200
West
East
Time 34 Myrs
Time 25 Myrs
Time 17 Myrs
0.1
Now a 200 ºC, thermal anomaly ponds under the lithosphere and the centre of extension jumps by 44 km to the west.
0
500
1000
1500
ºC
0.00
0.05
0.10
0.15
0.20
0.25
Melt Fraction
18
19
20
21
22
23
24
log10Pa s

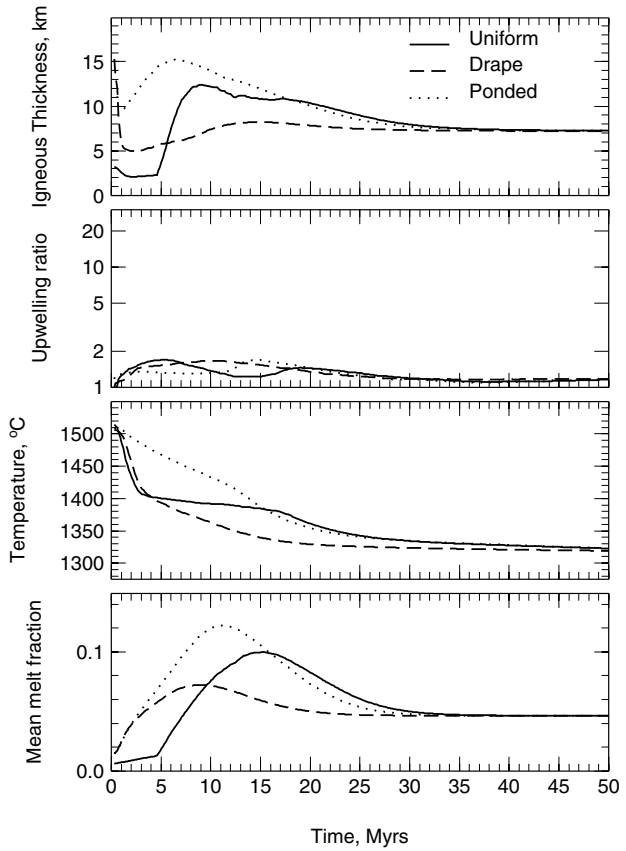
Igneous Thickness, km
Uniform
Drape
Ponded
Upwelling ratio
Temperature, °C
Mean melt fraction
Time, Myrs

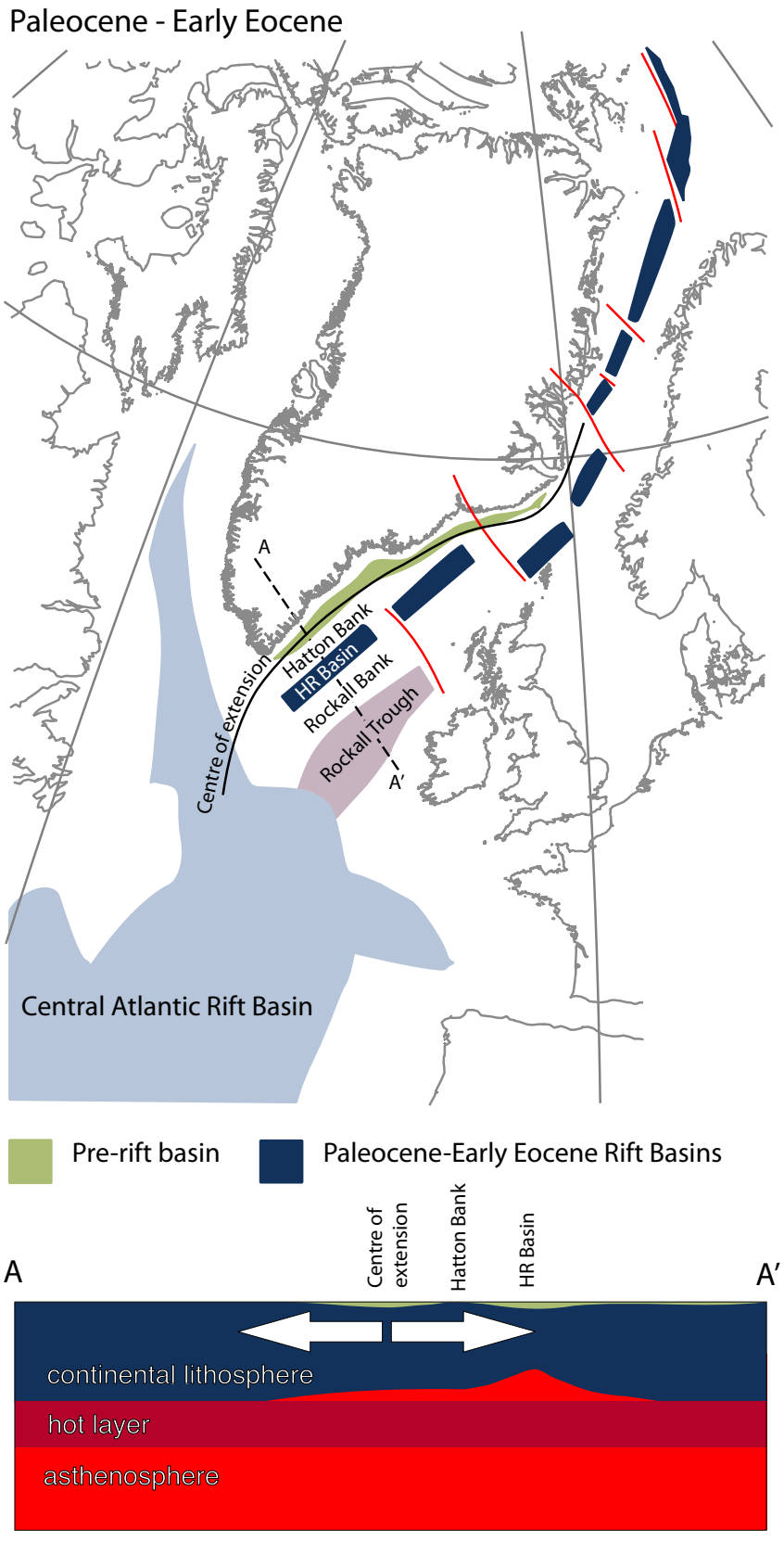
Paleocene - Early Eocene
A
Hatton Bank
HR Basin
Rockall Bank
Rockall Trough
A'
Centre of extension
Central Atlantic Rift Basin
Pre-rift basin
Paleocene-Early Eocene Rift Basins
A
Centre of extension
Hatton Bank
HR Basin
A'
continental lithosphere
hot layer
asthenosphere

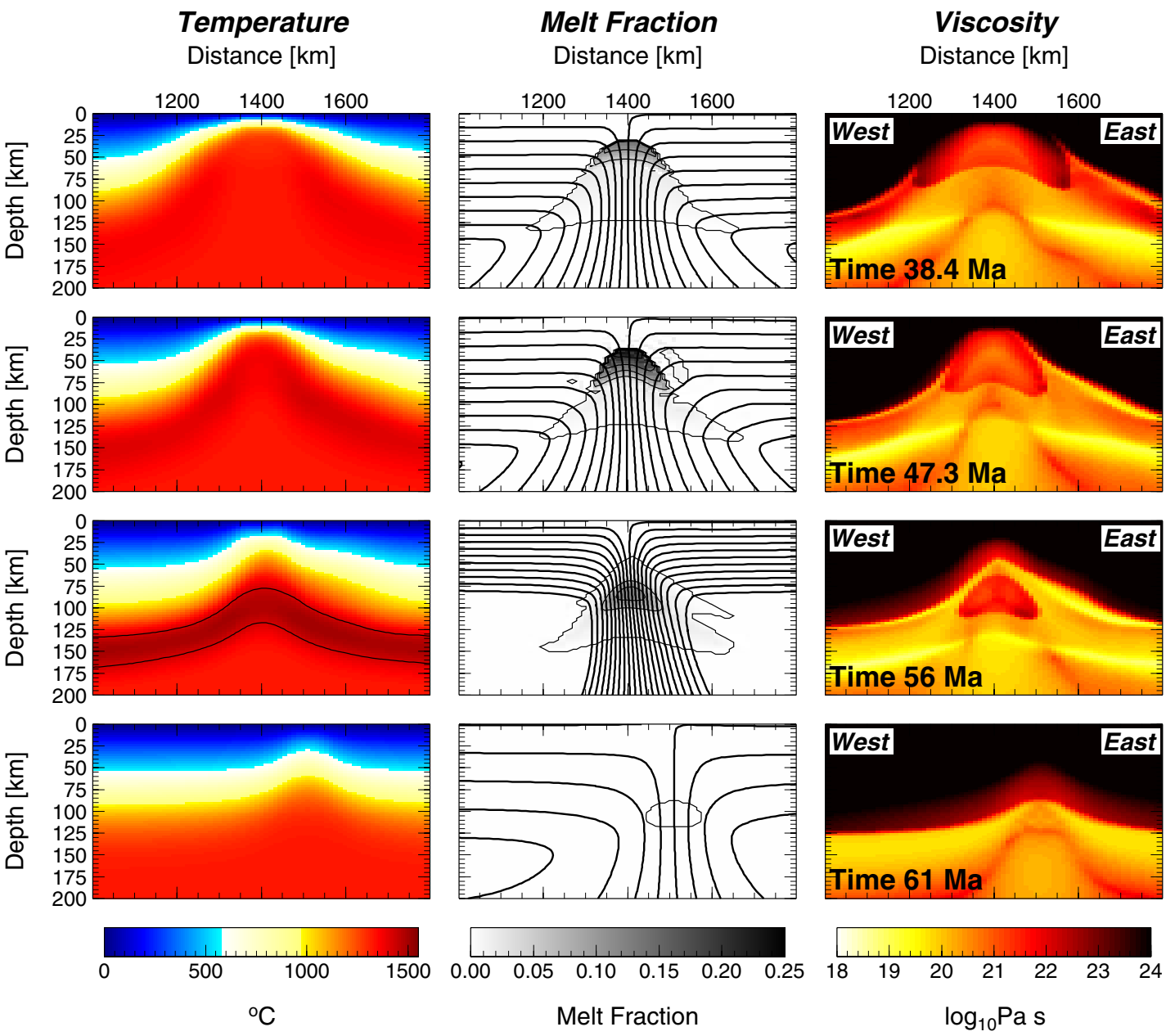
Temperature
Melt Fraction
Viscosity
Distance [km]
1200
1400
1600
Depth [km]
0
25
50
75
100
125
150
175
200
West
East
Time 38.4 Ma
Time 47.3 Ma
Time 56 Ma
Time 61 Ma
0
500
1000
1500
°C
0.00
0.05
0.10
0.15
0.20
0.25
Melt Fraction
18
19
20
21
22
23
24
log10Pa s

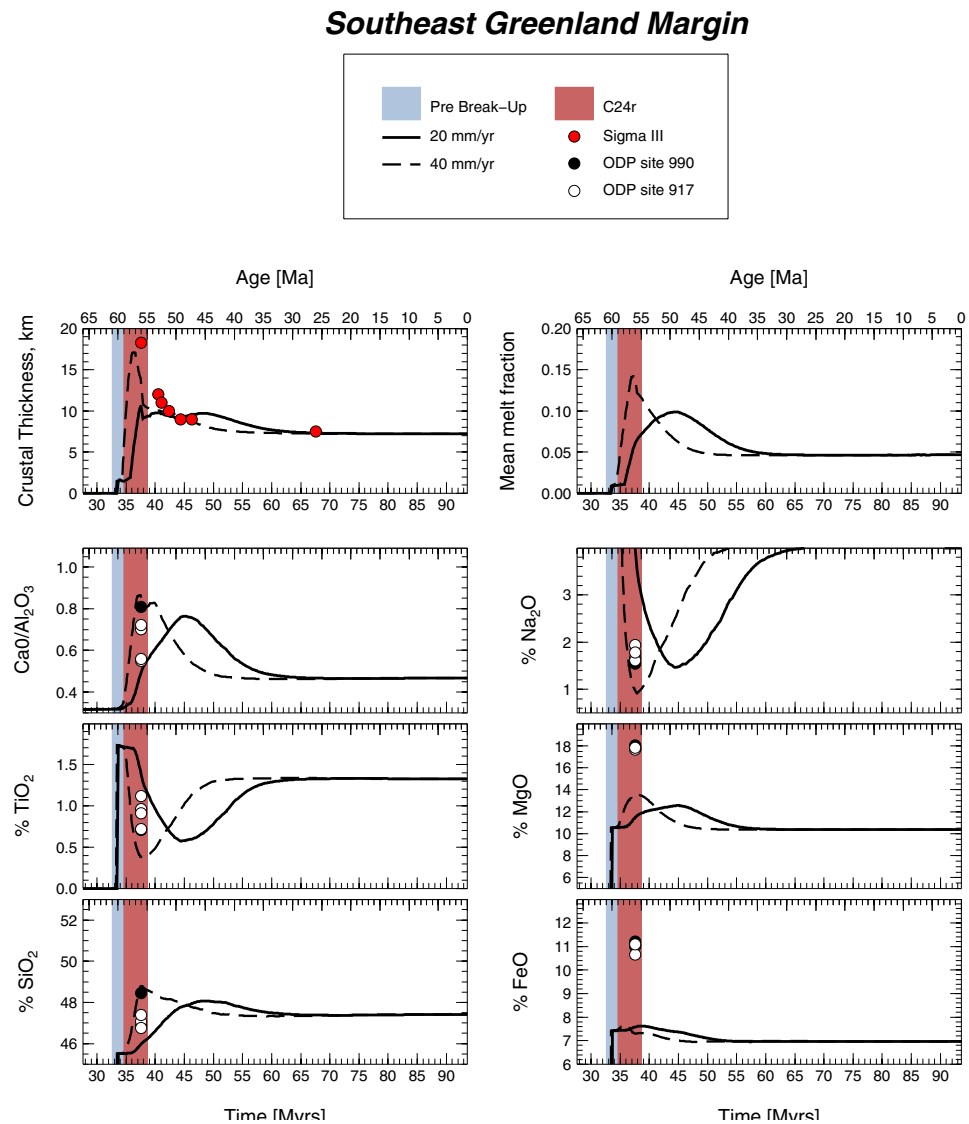
Southeast Greenland Margin
Pre Break-Up
C24r
20 mm/yr
Sigma III
ODP site 990
ODP site 917
Age [Ma]
Age [Ma]
Crustal Thickness, km
Mean melt fraction
Ca0/Al2O3
% Na2O
% TiO2
% MgO
% SiO2
% FeO
Time [Myrs]
Time [Myrs]